Stem Cell Reports
Article

ISSCR

OPEN ACCESS

# Distinct Phases of Postnatal Skeletal Muscle Growth Govern the Progressive Establishment of Muscle Stem Cell Quiescence

Francesca Gattazzo,[1] Béatrice Laurent,[1] Frédéric Relaix,[1,2,3,*] Hélène Rouard,[1] and Nathalie Didier[1,*]
[1]Univ Paris Est Creteil, INSERM, EFS, IMRB, Creteil 94010, France
[2]EnvA, IMRB, Maisons-Alfort 94700, France
[3]AP-HP, Hopital Mondor, Service d'Histologie, Creteil 94010, France
*Correspondence: frederic.relaix@inserm.fr (F.R.), nathalie.didier@inserm.fr (N.D.)
https://doi.org/10.1016/j.stemcr.2020.07.011

## SUMMARY

Muscle stem cells (or muscle satellite cells [MuSCs]) are required for postnatal growth. Yet, the detailed characterization of myogenic progression and establishment of quiescence during this process remains poorly documented. Here, we provide an overview of myogenic cells heterogeneity and dynamic from birth to adulthood using flow cytometry. We demonstrated that PAX7+ cells acquire an increasing ability to progress in the myogenic program from birth to adulthood. We then simultaneously analyzed the cycling state (KI67 expression) of the MuSCs and progenitors (PAX7+) and their progression into myogenic precursors (PAX7−MYOD+) and differentiating cells (MYOG+) *in vivo*. We identified two distinct peaks of myogenic differentiation between P7–P10 and P21–P28, and showed that the quiescent MuSC pool is established between 7 and 8 weeks of age. Overall our study provides a comprehensive *in vivo* characterization of myogenic heterogeneity and demonstrates the highly dynamic nature of skeletal muscle postnatal growth process.

## INTRODUCTION

Adult skeletal muscle contains quiescent myogenic stem cells or satellite cells (MuSCs) anatomically defined by their specific location between the sarcolemma and the basal lamina of the myofiber (Katz, 1961; Mauro, 1961). During development, myogenic progenitors expressing both PAX3 and PAX7 proceed to embryonic and fetal myogenesis (Gros et al., 2005; Kassar-Duchossoy et al., 2005; Relaix et al., 2005). These PAX3+PAX7+ progenitors initiate the lineage progression through the myogenic differentiation program by sequentially expressing the myogenic regulatory factors (MRFs) MYF5, MRF4, MYOD, and myogenin (MYOG), leading to the formation and growth of the myofibers during embryonic and fetal development (Gros et al., 2005; Kassar-Duchossoy et al., 2005; Relaix et al., 2005; Rudnicki et al., 1993; Tapscott, 2005). Furthermore, at the late stage of fetal development these resident progenitors were shown to contribute to the formation of the basal lamina and adopt the characteristic sub-laminal position of the satellite cells (Bröhl et al., 2012; Gros et al., 2005; Kassar-Duchossoy et al., 2005; Relaix et al., 2005). Interestingly, genetic ablation of MYOD-expressing cells in the embryo led to an almost complete loss of PAX7+ progenitors at embryonic day 12.5 (E12.5) and further at E16.5 indicating that the majority of these emerging satellite cells went through a transient MYOD+ stage (Wood et al., 2013). Although it remains unclear whether all emerging satellite cells have undergone the myogenic program, i.e., expressed MYF5 and/or MYOD during development (Relaix and Zammit, 2012), part of them (15%–20%) proliferate and are therefore likely to participate in myofibers growth during perinatal and postnatal periods (Bröhl et al., 2012; White et al., 2010). Studies in chick and mouse described the co-existence of a predominant fast-cycling PAX7+MYF5+ population and a smaller slow-cycling PAX7+MYF5− population throughout embryonic and fetal development (Picard and Marcelle, 2013). During fetal development (E15), a portion of both PAX7+MYF5+ and PAX7+MYF5− populations exits the cell cycle (20% and 50%, respectively), monitored by KI67 expression, suggesting that a pool of quiescent satellite cells is already established at the end of fetal development (Picard and Marcelle, 2013).

After birth, skeletal muscle growth is characterized by extensive morphological and metabolic changes (Bachman et al., 2018; Pala et al., 2018; White et al., 2010). Until recently, it was commonly accepted that, until the weaning age (postnatal day 21 [P21]) myofibers increase in size by the addition of new myonuclei, or myonuclear accretion, supported by the proliferation of PAX7+ cells (Bachman et al., 2018; White et al., 2010). During this process, the overall number of PAX7+ cells gradually declines and at P21 cycling PAX7+ progenitor cells become mitotically quiescent while the number of quiescent MuSCs and myonuclei become stabilized as in the adult (Lepper et al., 2009; White et al., 2010). Thereafter and until young adulthood (P56), further muscle growth was considered independent from myonuclear accretion and mainly achieved by myofiber hypertrophy (Lepper et al., 2009; Stantzou et al., 2017; White et al., 2010). However, different groups recently reported that nuclear accretion sustained by PAX7+ cells was prolonged until the pre-pubertal age (Bachman et al., 2018; Kim et al., 2016), and that cycling PAX7+ cells were still present at this stage underlying that complete establishment of

quiescent MuSC pool might happen at later stages of the postnatal growth (Bachman et al., 2018; Kim et al., 2016). Likewise, Bachman et al. (2018) observed that the number of MuSCs in the extensor digitorum longus (EDL) and soleus muscles stabilized at 8 weeks. Importantly, cell-cycle inhibitors and sex hormones have been shown to trigger the transition from proliferative juvenile myogenic progenitors to quiescent MuSCs (Chakkalakal et al., 2014; Kim et al., 2016; Sato et al., 2014). However, the dynamics of postnatal growth, as well as the precise moment in which complete quiescence is achieved, are still unclear.

Adult MuSCs are necessary for adult muscle homeostasis and regeneration after injury (Lepper et al., 2011; McCarthy et al., 2011; Murphy et al., 2011; Sambasivan et al., 2011; White et al., 2010). In response to muscle damage, quiescent MuSCs activate, re-enter the cell cycle and proliferate. Dividing PAX7+ cells can either differentiate and subsequently fuse to form new muscle fibers or repair damaged fibers, or self-renew to progressively restore the pool of quiescent MuSCs (Chargé and Rudnicki, 2004; Relaix and Zammit, 2012; Zammit et al., 2004). These different stages of adult myogenesis have been extensively studied by *ex vivo* experiments, namely in isolated single fibers or purified-MuSCs cultured in high mitogenic conditions, by monitoring the expression of the specific markers: PAX7, MYOD (activation), and MYOG (differentiation). In brief, upon withdrawal from their natural niche, quiescent PAX7+MYOD− MuSCs rapidly activate (Machado et al., 2017), and give rise to proliferating PAX7+MYOD+ myoblasts. Most of these PAX7+MYOD+ myoblasts commit to differentiation by downregulating PAX7 and expressing MYOG. A small proportion of these myoblasts maintain PAX7 while downregulating MYOD, exit the cell cycle, and return in a quiescent state (self-renewal) (Kuang et al., 2007; Machado et al., 2017; Zammit et al., 2002, 2004).

In contrast to adult myogenesis, a detailed characterization of the dynamics of myogenic cells and their cycling status during postnatal growth is missing mainly due to technical limitations. Based on current knowledge, the pool of myogenic cells is likely highly heterogeneous and dynamic at birth as well as during the early stages of postnatal growth, presumably, including (1) quiescent MuSCs, (2) dividing PAX7+ cells co-expressing MYOD that will progress toward differentiation or quiescence, and (3) differentiating PAX7−MYOG+ cells. Therefore, we first compared the *in vitro* behavior of the myogenic cells purified from the CD45$^-$TER-119$^-$CD31$^-$SCA-1$^-$CD34$^+$ITGA7$^+$ fraction (referred to as the CD34$^+$ITGA7$^+$ fraction) at three different stages of early postnatal growth (P0, P7, and P15) and in adulthood (P56). We found that upon *in vitro* expansion in high mitogenic conditions, P0-derived myogenic cells were less prone to spontaneously commit to myogenic differentiation compared with those purified at later time points. Accordingly, P15-derived myogenic cells were more fusogenic than their younger counterparts while P56-derived myogenic cells showed the strongest tendency to terminally fuse. Furthermore, we performed a detailed *in vivo* characterization of the evolution of myogenic cell populations from birth to adulthood in terms of their reciprocal composition (PAX7+, MYOD+, and MYOG+), their cycling state (KI67 expression), and the establishment of the quiescent MuSC pool by flow cytometry. Based on our observation, we clarified the progression of the myogenic populations into the myogenic differentiation program during postnatal growth. Our study provides a qualitative and quantitative analysis of myogenesis from birth to adulthood and identifies distinct phases of growth, differentiation, and establishment of MuSC quiescence. In addition, we demonstrated that the distinct *in vitro* behavior of PAX7+ cell-derived myoblasts was determined by their intrinsic properties elicited by the different phases of the postnatal growth process.

## RESULTS

### Composition and *In Vitro* Behavior of CD34$^+$ITGA7$^+$ Myogenic Fractions Dynamically Change from Birth to Adulthood

CD34 and α7-integrin (ITGA7) are surface markers commonly used to purify PAX7+-enriched myogenic fraction from postnatal and adult muscles (Gromova et al., 2015; Maesner et al., 2016; Pasut et al., 2012). Whereas in homeostatic adult muscle, quiescent PAX7+ MuSCs are predominant, the composition of the CD34$^+$ITGA7$^+$ myogenic fraction is more likely to evolve with postnatal growth dynamic process. Hence, we investigated the relative proportions of PAX7+, MYOD+, and MYOG+ cells in CD34$^+$ITGA7$^+$ fraction from newborn (P0), 1-week-old (P7), 2-week-old (P15), and 8-week-old (P56) mouse hindlimb muscles by flow cytometry (Figures 1A–1C, S1A, and S1B; Table S1). In adult muscle, the CD34$^+$ITGA7$^+$ fraction exhibited mainly PAX7+ cells (83%), while MYOD+ and MYOG+ cells were rarely detected. Of note, the digestion process was longer for P56 muscles than for postnatal muscles (see Experimental Procedures). Given our recent observation (Machado et al., 2017), we must report that the percentage of PAX7+ cells observed for adult muscle may be slightly underestimated due to PAX7 protein degradation and/or downregulation during digestion. Conversely, in postnatal muscles, the CD34$^+$ITGA7$^+$ fraction consisted of a mixed population, including PAX7+, MYOD+, and MYOG+ cells, the proportion of which changed over time (Figures 1B and 1C). We thus sought to compare the behavior of the myogenic cells purified from the CD34$^+$ITGA7$^+$ fraction of P0, P7, P15, and P56 muscles upon *in vitro* expansion. We plated the cells at

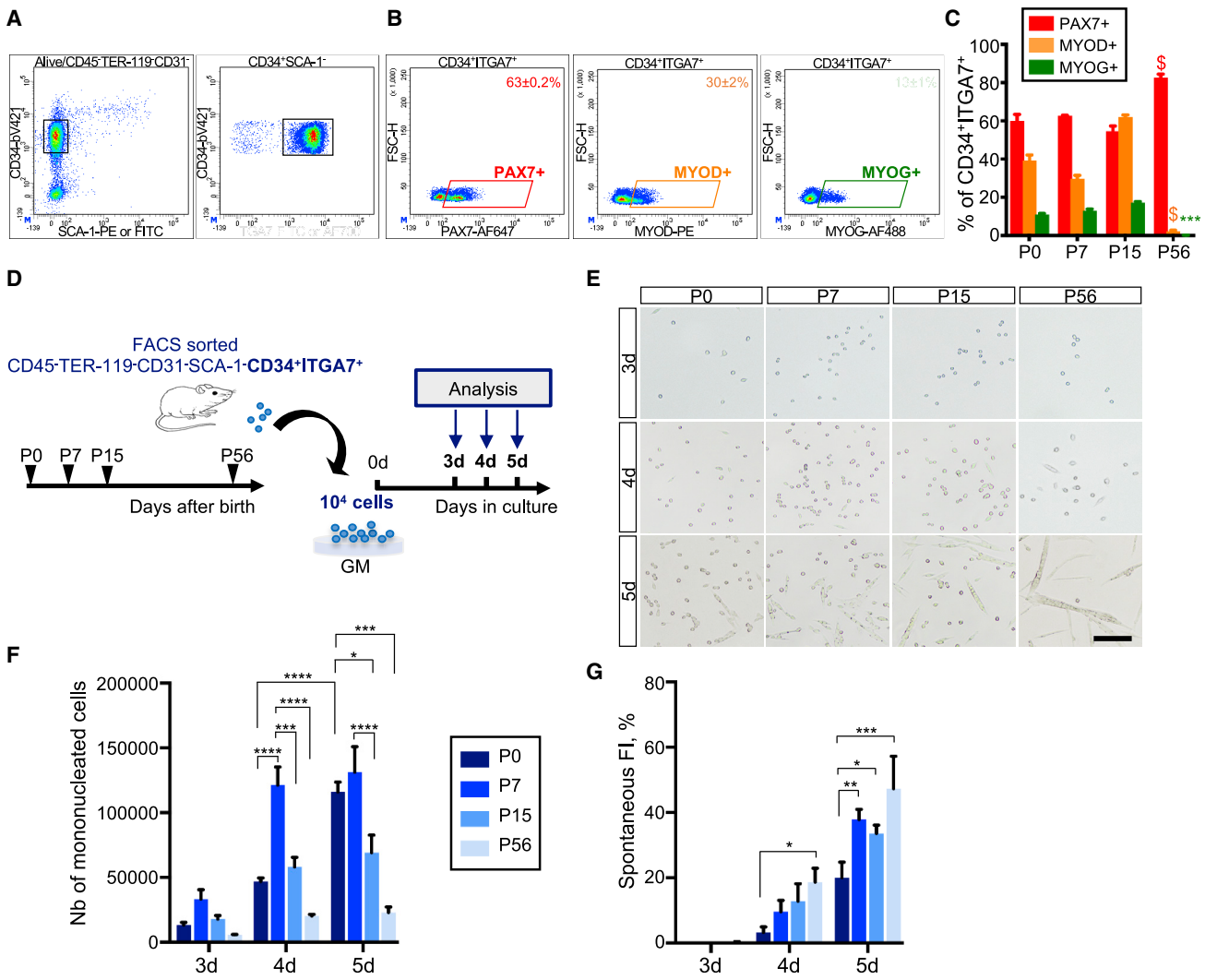


**Figure 1. Distinct Composition and *In Vitro* Behavior of Myogenic Cells of the CD34$^+$ITGA7$^+$ Fraction of Postnatal or Adult Muscles**

(A and B) Representative density scatterplots showing the gating strategy used to determine the proportion of PAX7+, MYOD+, and MYOG+ cells among the CD45$^-$TER-119$^-$CD31$^-$SCA-1$^-$CD34$^+$ITGA7$^+$ fraction (referred to as CD34$^+$ITGA7$^+$ fraction) from P7 mouse muscles. (A) Debris, doublets, CD45$^+$TER-119$^+$CD31$^+$, and dead cells were excluded from the analysis (Figure S1; Table S1) and ITGA7$^+$ cells were gated from the CD34$^+$SCA-1$^-$ fraction. (B) Gates used to determine the proportion of PAX7+, MYOD+, and MYOG+ cells.

(C) Bar graph showing the proportion of PAX7+, MYOD+, and MYOG+ cells. Two-way ANOVA analysis, with ***$p < 0.001, \$p < 0.0001$ relative to P0.

(D) Purified CD34$^+$ITGA7$^+$ cells were plated at the same density and cultured in growth medium for 3, 4, and 5 days.

(E–F) (E) Optical micrographs of cultured-myogenic cells. Scale bar, 100 μm. Quantification of (F) the total number of mononucleated cells, (G) their spontaneous fusion index, calculated as number of nuclei incorporated in myotubes on total number of nuclei per field. Values are represented as the mean ± SEM of three independent experiments (n = 3 mice/group). Two-way ANOVA analysis, with *$p < 0.05$, **$p < 0.01$, ***$p < 0.001$, ****$p < 0.0001$.

the same density and cultured them under conditions allowing efficient expansion and spontaneous fusion from 3 to 5 days (Danoviz and Yablonka-Reuveni, 2012; Montarras et al., 2005) (Figures 1D–1G). We compared the amplification rate of the cells by quantifying the total number of mononucleated cells obtained after trypsinization (Figures 1E and 1F). After 3 days of culture, the total number of mononucleated cells was statistically similar between P0, P7, P15, and P56. However, after 4 days, P7 cells were significantly more abundant than P0, P15, and P56 cells. Whereas the number of P0 cells progressively increased between 4 and 5 days of culture, the number of P7, P15, and P56 cells remained equivalent (Figure 1F). Indeed, after 5 days the total number of P0 cells was almost 9-fold higher than observed at 3 days, while the number of P7, P15, and P56 cells was increased by only 4-fold (Table S2). By

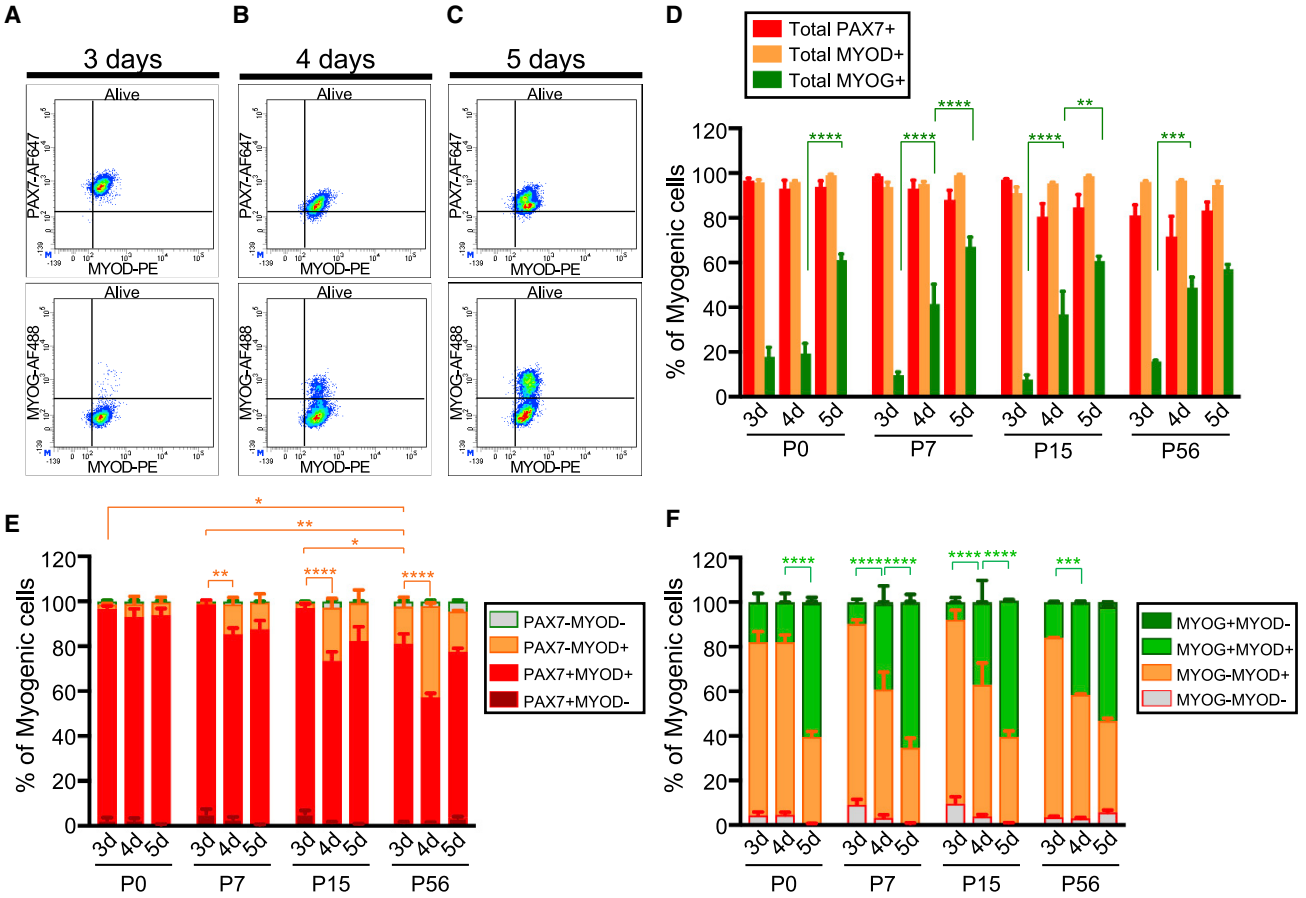


**Figure 2. Increasing Ability of Cultured-Myogenic Cells of the CD34$^{+}$ITGA7$^{+}$ Fraction to Progress in the Differentiation Program**

(A–F) (A–C) Representative density scatterplots showing the repartition of PAX7/MYOD (upper panel), MYOD/MYOG (lower panel) expression in cultured-myogenic cells. Debris and dead cells were excluded from the analysis. Gates were positioned based on FMO controls (Figures S2F and S2G). Graphs showing (D) the relative proportion of total PAX7+, MYOD+, and MYOG+ cells, and the repartition of (E) PAX7/MYOD and (F) MYOD/MYOG expression. Values are the mean ± SEM of three independent experiments (n = 3 mice/group). Statistical significance is represented relative to PAX7−MYOD+ cells (E) or MYOD+MYOG+ cells (F). Two-way ANOVA analysis, with *p < 0.05, **p < 0.01, ***p < 0.001, ****p < 0.0001.

quantifying the spontaneous fusion events, we noticed that this prolonged expansion of P0 cells may mainly rely on their reduced propensity to fuse compared with their later postnatal and adult counterparts. While we observed a reduced number of mononucleated cells for P15 and P56 cells compared with P7 cells, their spontaneous fusion index was equivalent, suggesting a higher tendency to fuse (Figure 1G). Altogether these observations suggest that myogenic cells of the CD34$^{+}$ITGA7$^{+}$ fraction of P0 muscle exhibit a reduced fusion potential compared with their later counterparts and that the *in vitro* fusogenicity of these cells increases from birth to adulthood.

To decipher further whether these distinct behaviors were due to intrinsic differences in myogenic cells or to the different initial composition of the CD34+ITGA7+ fractions, we compared the expression profiles of specific markers during culture (Figure 2). To this aim, we developed a strategy to simultaneously analyze PAX7, MYOD, and MYOG by flow cytometry (Figures 2A–2C). We verified the specificity of the coupled antibodies (listed in Table S3) by performing the corresponding isotypic controls (Figure S2A). In addition, we used fluorescence-activated cell sorting (FACS) to sort cells stained with these coupled antibodies and counterstained them with antibodies commonly used for immunofluorescence (IF) in the field (Figures S2B–S2D; Table S4) (Eliazer et al., 2019; Machado et al., 2017; Paris et al., 2016). Finally, we confirmed that endogenous PAX7 expression analyzed with coupled anti-PAX7-AF647 antibody correlated with GFP expression in myogenic cells derived from *Tg:PAX7-nGFP* mouse muscles (Figure S2E). We took advantage of this method to define the relative proportion of total PAX7+, total MYOD+, and

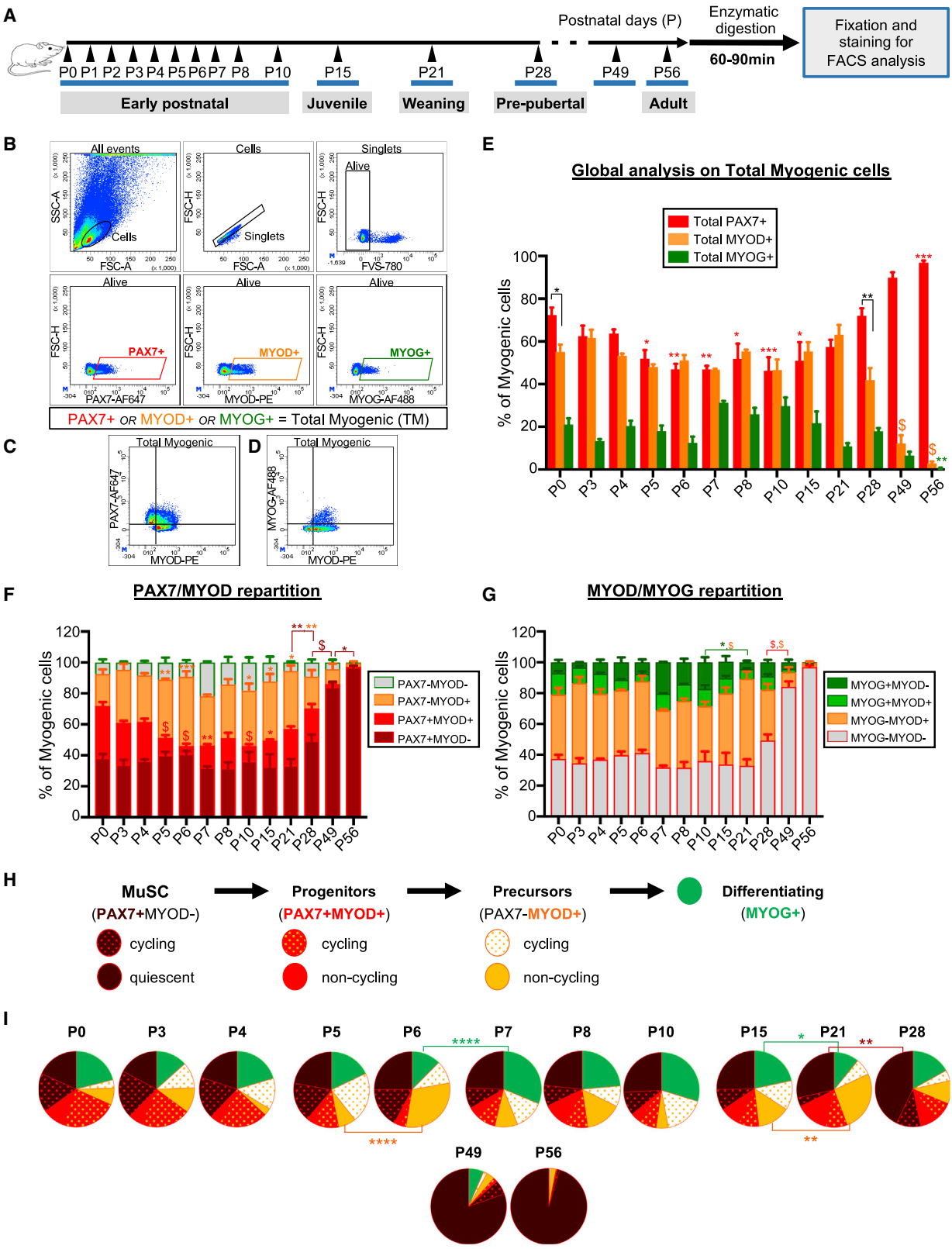


*(legend on next page)*

total MYOG+ cells (Figure 2D), the repartition of the myogenic cells in terms of PAX7/MYOD (Figure 2E) and MYOD/MYOG (Figure 2F) expression. Our global analysis showed that, in our culture conditions, nearly all the mononucleated cells were PAX7+ and/or MYOD+. Moreover, cultured cells progressively underwent differentiation between 3 and 5 days, reaching statistically equivalent final proportion of differentiating MYOG+ cells at 5 days (57% for P56 to 67% for P7) (Figure 2D). A deeper analysis revealed that, although derived from $CD34^{+}ITGA7^{+}$ fraction with distinct composition, after 3 days of culture nearly all postnatal P0, P7, and P15 cells were PAX7+MYOD+ (Figure 2E). This observation suggested that committed PAX7–MYOD+ and differentiating MYOG+ cells were lost upon seeding and that the differential behavior observed *in vitro* depended exclusively on the initial pool of PAX7+ cells. Then, P7 and P15 cells progressively differentiated between 3 and 5 days of culture, as shown by the significant increase in the proportion of MYOG+MYOD+ cells (Figure 2F). However, in accordance with our previous observations (Figures 1F and 1G), we noted that for P0 cells the proportion of MYOG+MYOD+ cells did not change between 3 and 4 days of culture indicating a delayed progression in the differentiation program compared with their later postnatal counterparts. Conversely, P56 cells differentiated faster as shown by the presence of committed PAX7–MYOD+ cells already after 3 days and the unchanged proportion of differentiating MYOG+MYOD+ between 4 and 5 days of culture (Figures 2E and 2F). Furthermore, we noticed that the MYOG mean level of expression progressively increased between 3 and 5 days of culture for P0 and P7 cells (Figure S2H). In contrast, the maximum level of MYOG expression in P15 and P56 cells was reached as early as 4 days of culture, suggesting that these cells progressed more rapidly in the myogenic differentiation program than P0 and P7 cells (Figure S2H).

To further validate our flow cytometry method, we performed similar analyses by the classical IF approach (Figures S3A, S3B, and S3F). These analyses confirmed that P0 cells displayed a delay in their commitment to differentiation compared with P15 and P56 cells and that P56 cells were the most prone to progress in the myogenic differentiation program upon *in vitro* expansion (Figures S3C–S3E). Nevertheless, we noted significant differences in the proportions of PAX7+ and MYOG+ determined by IF and flow cytometry. In particular, we observed an unexpectedly higher overlap between PAX7- and MYOG-expressing cells by flow cytometry than by IF. Given that in our conditions of culture we observed the presence of double-positive PAX7+MYOG+ cells by IF (Figures S3G and S3H), we assumed that these discrepancies mainly relied on the higher sensitivity of flow cytometry that allowed a better detection of cells expressing low levels of PAX7 and/or MYOG. This higher sensitivity, combined with the possibility to analyze simultaneously the expression of the three markers PAX7, MYOD, and MYOG in a larger amount of cells, demonstrated that flow cytometry analysis is a powerful and reliable strategy for the characterization of myogenic cell behavior *in vitro*.

Overall these results demonstrated that PAX7+ myogenic cells display intrinsic differences during postnatal growth and in the adult when expanded *in vitro*. In particular, these cells acquire a higher ability to progress in the myogenic program and have an increased fusogenicity from birth to adulthood.

## Analysis of Myogenic Cell Dynamics *In Vivo* from Birth to Adulthood by Flow Cytometry

We hypothesized that the intrinsic differences observed between postnatal and adult myogenic cells during *in vitro* expansion may correspond to different phases of the postnatal growth process *in vivo*. We thus transposed our flow cytometry method to evaluate the behavior of the myogenic populations during postnatal growth. We analyzed the mononucleated cells from digested mouse hindlimb muscles isolated at different ages: newborn (P0), early postnatal (P0–P7, P8, and P10), juvenile (P15), weaning (P21), pre-pubertal (P28), and young adult (P49 and P56) (Figure 3A). Cells were fixed immediately after enzymatic digestion and immunostained for PAX7, MYOD, and MYOG simultaneously. We performed all our analyses on the total myogenic population (considered as 100%), defined as the sum of the cells that were expressing

**Figure 3. *In Vivo* Characterization of the Myogenic Populations from Birth to Adulthood**

(A) Experimental timeline.

(B–G) (B) Strategy of analysis. Debris, doublets, and dead cells were excluded from the analysis. Representative density scatterplots showing the gates used to analyze myogenic cells in P7 mouse muscles. Joined gate PAX7+ or MYOD+ or MYOG+ cells was considered as the total myogenic cells (100%) referred to as TM. Representative density scatterplots showing, the repartition of (C) PAX7/MYOD and (D) MYOD/MYOG expression on TM (see also Figures S4A and S4B). Graphs showing (E) the proportion of total PAX7+, MYOD+, and MYOG+ cells, and the repartition of (F) PAX7/MYOD and (G) MYOD/MYOG expression on TM.

(H) Analysis of the myogenic cells was refined based on their cycling state, monitored by KI67 expression.

(I) Pie charts showing the distribution and the cycling state of the myogenic populations. Values represent the mean of data obtained from three to eight mice for each time point. Statistical significance is shown in Tables S5 and S6. Two-way ANOVA analysis, with *$p < 0.05$, **$p < 0.01$, ***$p < 0.001$, $ or ****$p < 0.0001$.

at least one of the markers PAX7, MYOD, or MYOG gated on the relative FMO (Figures 3B–3D and S4B). We evaluated the composition of the global myogenic population (Figure 3E), and the repartition of PAX7/MYOD and MYOD/MYOG expression (Figures 3F and 3G).

From our global analysis we observed that, between P0 and P21, PAX7+ and MYOD+ cells represented nearly all the myogenic cells, whereas the proportion of MYOG+ cells remained less abundant (11% at P21 to maximum 31% at P7). While at birth the percentage of PAX7+ cells was slightly higher than that of MYOD+ cells, between P3 and P21 their global proportion was equivalent. From P28, we observed a significant reduction in the proportion of MYOD+ (42%) compared with PAX7+ cells (72%). Between P49 and P56, the proportion of PAX7+ cells reached 97% of the total myogenic cells, while the proportion of MYOD+ and MYOG+ cells strongly decreased and became almost undetectable at P56 (Figure 3E; Table S5).

By analyzing the relative distribution of PAX7+ and MYOD+ cells on total myogenic cells, we found that at birth the proportion of PAX7+ cells was equally divided in PAX7+MYOD− and PAX7+MYOD+ cells, whereas we detected a minor proportion of committed PAX7−MYOD+ or differentiating PAX7−MYOD− cells corresponding to MYOG+MYOD− cells (Figures 3F and 3G). Between P0 and P21, the proportion of PAX7+MYOD− cells was stable at about 40%. During this period, the proportion of PAX7+MYOD+ cells was significantly reduced between P5 and P15 compared with P0 concomitantly to an increased proportion of committed PAX7−MYOD+ cells at P5 and P6, and then between P10 and P15. Between P10 and P21, the proportion of the differentiating MYOG+MYOD− cells progressively declined, likely resulting from the terminal fusion of these cells with myofibers. Finally, from P28 the proportion of PAX7+MYOD− cells significantly increased to reach 97% of the total myogenic population between P49 and P56 consistently with the completion of the postnatal growth process (Figures 3F and 3G; Table S5).

From this first set of analyses, we identified different phases during the postnatal growth process. In addition, we observed that the proportion of PAX7+MYOD− cells within the total myogenic population significantly increased from P28 and coincided with the total PAX7+ population after 7 weeks (P49) indicating that the definitive establishment of the quiescence was likely to occur during this period.

### Overview of the Myogenic Populations and Their Cycling State during Postnatal Growth to Adulthood

To better define the different phases of the postnatal growth emerging from our previous observations, we next included the KI67 marker to our analysis to distinguish cycling from non-cycling cells. Accordingly, we divided the myogenic populations into quiescent and cycling MuSCs (PAX7+MYOD−KI67− and PAX7+MYOD−KI67+), non-cycling and cycling progenitors (PAX7+MYOD+KI67− and PAX7+MYOD+KI67+), non-cycling and cycling precursors (PAX7−MYOD+KI67− and PAX7−MYOD+KI67+), and differentiating MYOG+ cells (Figures 3H, 3I, and S4C). We confirmed that between P0 and P4 the global myogenic composition was stable and that at this stage the pool of quiescent MuSCs already represented almost 20% of the total myogenic cells, in keeping with previous observations that quiescent MuSCs are already established during the late fetal period (Picard and Marcelle, 2013). By P5, the proportion of cycling progenitors was significantly reduced, with a parallel increase of the proportion of cycling precursors, followed at P6 by an important increase of the proportion of non-cycling precursors and differentiating MYOG+ cells between P7 and P10. We assumed that MYOG+ cells terminally fused since the proportion of MYOG+ cells was significantly reduced and almost disappeared at P21. As observed at P6, the proportion of non-cycling precursors increased between P15 and P21. We thus speculated that the phase of myogenic commitment observed at P21 was followed by a second wave of terminal differentiation between P21 and P28. Accordingly, at P28 the proportion of precursor cells was significantly reduced compared with P21 and the proportion of quiescent MuSCs started to increase. Afterward, we observed that from P49 quiescent MuSCs represent almost the totality of the myogenic cells (80%). However, a small proportion of cycling MuSCs (6%) was still detectable, demonstrating that the constitution of the quiescent MuSC pool was not completely achieved (Figure 3I; Table S6).

In summary, our data highlight different phases during postnatal growth. A first phase, between P0 and P4, during which the repartition of the myogenic populations is stable, that seems mainly dedicated to the amplification of the myogenic populations since 64% the total myogenic cells are cycling at P4. Then, PAX7+ progenitors undergo two successive commitment/differentiation waves between P7–P10 and P21–P28. In parallel, the quiescent MuSC pool accounting for ∼20% of the myogenic cells at P0 progressively increases after P28 (43%) to constitute almost the totality of the myogenic cells between P49 and P56.

### Quantification and Anatomical Location of the Myogenic Cells at Critical Stages of Postnatal Growth

To strengthen our study and investigate the anatomical location of MuSCs and progenitors during postnatal growth, we performed immunostaining for PAX7, MYOD, and MYOG markers on the tibialis anterior (TA) cross-sections at relevant time points: P0, P3, P7, P10, P15, P21, P28, and P56. Given the technical limitation of simultaneously monitoring the

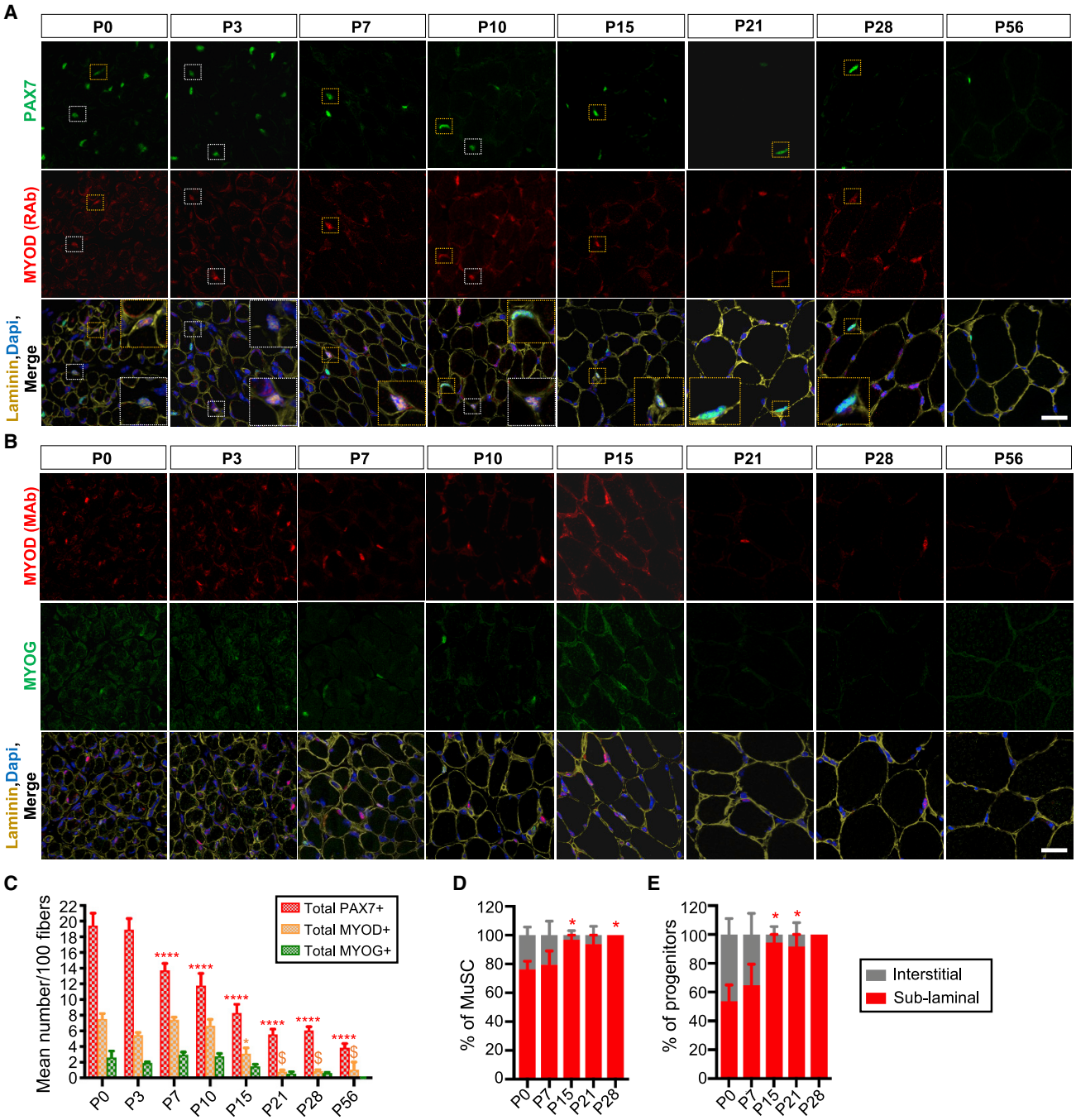


**Figure 4. Immunohistological Analysis of Myogenic Cells Location during Postnatal Growth**

(A and B) Representative tibialis anterior (TA) muscle cross-sections immunostained for (A) PAX7 (green), MYOD (red), and laminin (yellow), (B) MYOG (green), MYOD (red), and laminin (yellow) (see also Figure S5). Nuclei were stained with DAPI. Scale bar, 20 μm. (C–E) (C) Quantification of the number of PAX7+, MYOD+, and MYOG+ cells normalized per 100 fibers. Quantification of the proportion of sub-laminal and interstitial (D) MuSCs and (E) progenitors. Yellow and white magnification inlets indicate sub-laminal and interstitial PAX7+MYOD+ progenitors, respectively. Values are the mean ± SEM of data obtained from minimum three different mice for each time point. Two-way ANOVA analysis, with *p < 0.05, **p < 0.01, ***p < 0.001, $ or ****p < 0.0001 versus P0.

three markers and the laminin, we performed co-immunostaining for PAX7/MYOD and MYOG/MYOD (Figures 4A, 4B, and S5). We found a mean of 19 PAX7+ cells/100 fibers in the P0 muscle that remained unchanged in the P3 muscle. Then, the number of PAX7+ cells progressively reduced until it stabilized at an average of 6 PAX7+ cells/100 fibers between

P21 and P28, and finally decreased to roughly 4 PAX7+ cells/100 fibers at P56 in accordance with previous studies (Bachman et al., 2018). In parallel, the mean number of MYOD+ and MYOG+ cells/100 fibers remained stable between P0 and P10 (with a mean of 7 MYOD+ and 3 MYOG+ cells/100 fibers at P0), started to decrease from P15 compared with P0, and then became rarely detectable from P21 (Figure 4C).

We next further analyzed the location of PAX7+ cells, i.e., PAX7+MYOD− MuSCs and PAX7+MYOD+ progenitors, relative to the basal lamina (Figures 4A, 4D, and 4E). Between P0 and P7, the majority of the MuSCs and the progenitors (80% and 65%, respectively) were already localized below the basal lamina. At P15, the proportion of MuSCs and progenitors in a sub-laminal position significantly increased compared with P0 and reached 100% at P28 (Figures 4D and 4E).

### Detailed Study of PAX7+ Cells from Birth to Adulthood and Quiescent MuSC Pool Establishment

We next focused on the PAX7+ cells and their cycling state. We first performed immunostaining for PAX7 and KI67 on TA muscle sections (Figure 5A). As expected, macroscopic observation revealed that the total number of KI67+ cells and PAX7+ cells progressively reduced during postnatal growth. Although rare, cycling PAX7+KI67+ cells were still present in the pre-pubertal muscle (P28) before finally disappearing in the adult muscle. We quantified the number of cycling (PAX7+KI67+) and non-cycling (PAX7+KI67−) PAX7+ cells per 100 fibers and expressed the results as the proportion of PAX7+ cells (Figures 5B and 5C). Our results indicated that at birth almost 65% of the PAX7+ cells were cycling. Although this proportion was significantly reduced after P10 (49%) and progressively declined over time, at P28 around 29% of PAX7+ cells were still cycling. However, cycling PAX7+ cells were absent in P56 muscle (Figures 5A–5C).

We next took advantage of our flow cytometry analysis to determine the precise kinetic of establishment of the quiescent MuSC pool during postnatal growth (Figures 5D–5F). In agreement with IF analysis, we found that the proportion of cycling PAX7+ cells at birth was around 65% and progressively decreased during postnatal growth. In addition, we detected a significant decrease in the proportion of cycling PAX7+ cells starting from P6 (39%), which further reduced to 25% in the weaning and pre-pubertal ages. Interestingly, we noticed that 8% of the PAX7+ cells were still cycling at P49 (Figure 5E). We thus investigated at which stage MuSC quiescence was definitively established. Toward this aim, we refined the population of PAX7+ cells as quiescent and cycling MuSCs (PAX7+MYOD−MYOG−KI67− and PAX7+MYOD−MYOG−KI67+), and non-cycling and cycling progenitors (PAX7+MYOD+MYOG−KI67− and PAX7+MYOD+MYOG−KI67+, respectively) (Figure 5F). The initial pool of quiescent MuSCs represented 27% of the total PAX7+ cells. Between P0 and P4, the distribution of PAX7+ cells did not significantly change (Figure 5F; Table S7). At P5 and P6, we observed a significant decrease in the proportion of cycling progenitors and an increase in the proportion of quiescent MuSCs compared with birth. Based on our previous observations (Figures 3F–3I), we assumed that this increased proportion of quiescent MuSCs partly resulted from the reduction in progenitors that committed to differentiation and fueled the increase in precursors observed at P6 (Figures 3F–3I).

While the proportion of quiescent MuSCs was stably maintained between P6 and P21 (51% at P21), the proportion of non-cycling progenitors progressively increased with a first peak observed at P8 and a second at P21 after birth, consistent with the two waves of differentiation between P7–P10 and P21–P28 previously identified (Figure 3H). Then, at P28 the total proportion of MuSCs reached the mean of 77% of the total PAX7+ cells mainly due to an increase in the proportion of quiescent MuSCs representing 62% of the total PAX7+ cells. At P49, myogenic progenitors became undetectable and nearly all the PAX7+ cells were in a quiescent state by P56. From this flow cytometry analysis, we concluded that the pool of quiescent MuSCs was definitively stabilized between 7 and 8 weeks after birth.

## DISCUSSION

In this study, we made use of a flow cytometry strategy based on the simultaneous analysis of the markers of myogenic identity and progression into differentiation, PAX7, MYOD, MYOG, and the cycling marker KI67, to unravel the behavior of the myogenic lineage during postnatal growth. We demonstrate that this is a fast and sensitive strategy that overcomes some of the technical limitations of IF. In addition, our study provides a detailed analysis of the behavior and the relative proportions of MuSCs, progenitors, committed precursors, and differentiating cells from the early stages of postnatal growth until adulthood. As a notable drawback of our approach is that the results must be expressed as proportions on the total myogenic population, the implementation of this strategy of analysis with a quantitative method is currently under development. With such a method, we aim to provide a rapid and reliable tool to assess the myogenic dynamics undergoing *in vivo* physiologic or pathologic processes, including muscle growth and regeneration, neuromuscular diseases, or aging.

We followed the global evolution of the myogenic populations at each postnatal stage by simultaneously characterizing the proportion of quiescent and cycling MuSCs, non-cycling and cycling progenitors and committed precursors, and differentiating MYOG+ cells on the total myogenic population (Figure 6). In adult muscle, MuSCs are in a

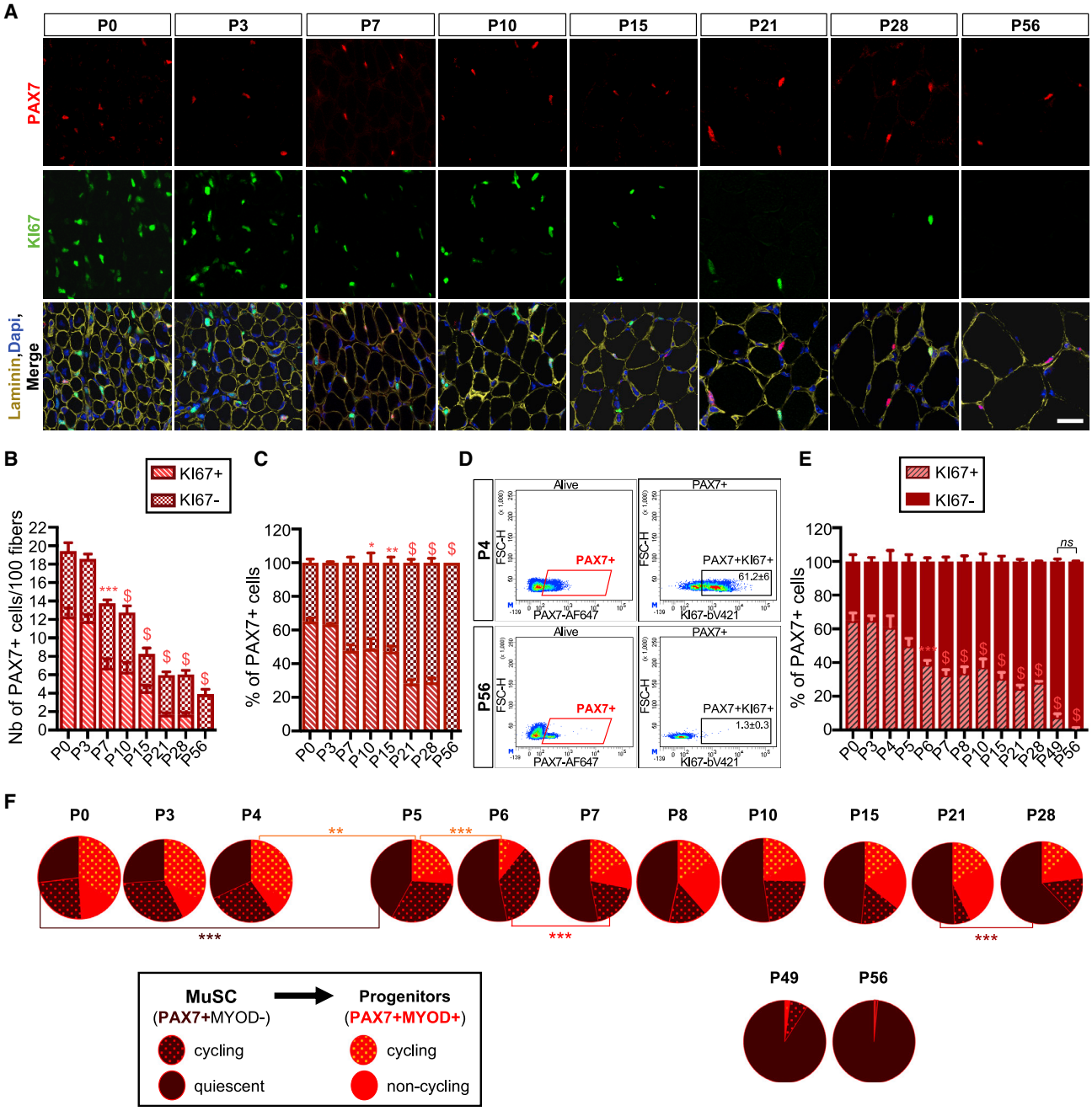


**Figure 5. Quiescent MuSC Pool Is Fully Established between P49 and P56**

(A–C) (A) Representative TA muscle cross-sections immunostained for PAX7 (red), KI67 (green), and laminin (yellow). Nuclei were stained with DAPI. Scale bar, 20 μm. Quantification of (B) the total number of cycling (KI67+) and non-cycling (KI67−) PAX7+ cells per 100 fibers, and (C) the proportion of cycling and non-cycling PAX7+ cells determined on TA cross-sections immunostained as in (A).

(D) Representative density scatterplots showing the gates used to determine the proportion of cycling PAX7+ cells by flow cytometry.

(E) Proportion of cycling and non-cycling PAX7+ cells obtained by flow cytometry.

(F) Pie charts showing the repartition of MYOD+ and KI67+ cells among total PAX7+ cells. Statistical significance is shown in Table S7. Values are the mean ± SEM of data obtained from three to eight mice for each time point. Two-way ANOVA analysis, with $p < 0.0001 versus P0.

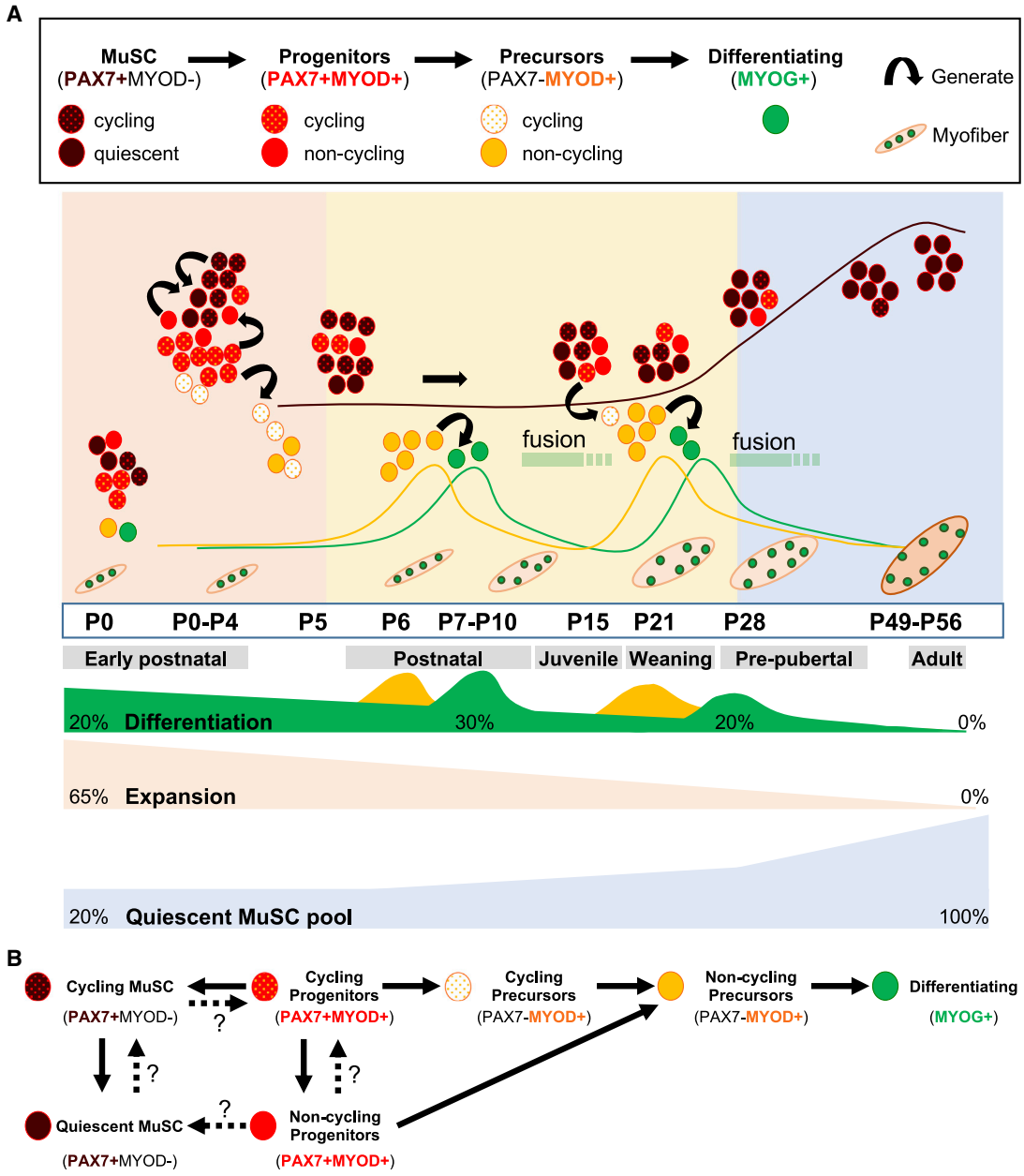


**Figure 6. Schematic Representation of Myogenic Cell Dynamics and Establishment of the Quiescent MuSC Pool during Muscle Postnatal Growth**

(A) Postnatal myogenesis is characterized by two successive phases of differentiation and progressive constitution of the quiescent MuSC pool.

(B) Proposed model for myogenic cell progression in the differentiation program during postnatal growth. Dotted lines represent fates of myogenic cells that remain to be investigated.

quiescent state, and upon activation (i.e., after injury) they undergo a well-established and coordinated program during lineage progression. Initially expressing MYOD during cycling, progenitors either commit to differentiation by downregulating PAX7 and expressing MYOG to provide additional myonuclei to myofibers, or downregulate MYOD to enter quiescence and reconstitute the quiescent MuSC pool (Kuang et al., 2007; Zammit et al., 2002, 2004). However, the dynamics and the composition of the myogenic cells governing early postnatal growth are not as well characterized. In line with previous observations during late fetal development (Picard and Marcelle,

2013), we show that neonatal muscles (P0–P4) possess a defined pool of quiescent MuSCs corresponding to ~20% of the total myogenic cells, and ~30% of the total PAX7+ cells. At these early stages, myogenic cells are mainly composed of cycling PAX7+MYOD− MuSCs and PAX7+-MYOD+ progenitors, and a less relevant proportion of committed PAX7−MYOD+ precursors and differentiated MYOG+ cells, suggesting that this period of the skeletal muscle postnatal growth is mostly dedicated to the amplification of the PAX7+ cells pool (Figure 6A). Thereafter, we identified two waves of myogenic differentiation between P7–P10 and P21–P28, preceded by an increase in the percentage of committed PAX7−MYOD+ precursors at P5–P6 and at P15–P21, respectively, followed by terminal differentiation and fusion. Our data are consistent with recent findings from Bachman et al. (2018) showing that PAX7+ cells continue to terminally fuse and increase myofiber CSA between 4 and 6 weeks and until 12 weeks after birth in the soleus and EDL muscles. From P28, the proportion of quiescent MuSCs significantly increases to represent almost the totality of the total myogenic cells between 7 and 8 weeks. In an attempt to better understand the respective behavior of the PAX7+ cells, namely the PAX7+MYOD− MuSCs and the PAX7+MYOD+ progenitors, we assessed the anatomical location and the cycling state of these cells from birth to adulthood. In accordance with recent findings, we confirmed that the definitive establishment of the quiescent MuSC pool is not achieved at P21 since ~30% of the total PAX7+ cells corresponding to ~19% of the MuSCs were still cycling at P28, namely at the pre-pubertal stage (Kim et al., 2016; Verma et al., 2018). Indeed, we demonstrate that the constitution of the adult quiescent MuSC pool is completed between P49 and P56. Interestingly, we noticed that from P28 all the PAX7+ cells, including quiescent and cycling MuSCs and non-cycling and cycling PAX7+MYOD+ progenitors, were located in a "satellite cell-like" sub-laminal position raising the question of their respective fate (Figure 6B). It seems reasonable to assume that most of the cycling MuSCs will finally exit the cell cycle and directly fuel the quiescent MuSC pool. Whether all the emerging MuSCs had at some point of skeletal muscle development expressed MYOD remains unclear mainly due to limitations in lineage-tracing animal models (for review see Relaix and Zammit, 2012). Nevertheless, previous observations showing that ablation of MYOD+-expressing cells during development induces the loss of nearly all PAX7+ cells, strongly support the view that the vast majority of MuSCs go through a transient MYOD+ state (Wood et al., 2013). Another uncertainty concerns the fate of the non-cycling PAX7+MYOD+ progenitors that could either downregulate MYOD and enter quiescence, or give rise to non-cycling committed precursors to provide additional myonuclei. However, since we observed that the absolute number of PAX7+ cells/100 fibers decreases by 33% between P28 and P56 in agreement with a recent study (Bachman et al., 2018), we assumed that non-cycling progenitors will rather commit to differentiation and fuse.

In addition to these *in vivo* experiments, we demonstrated that $CD34^{+}ITGA7^{+}$ myogenic cells isolated at different postnatal ages had a differential behavior upon *in vitro* expansion. Indeed, we showed that myoblasts derived from newborn muscle (P0) have a prolonged expansion rate and a delay in their commitment to differentiation compared with those isolated at later stages of postnatal growth (P7 and P15) and adulthood. Conversely, we noted that P15 and P56 myoblasts had a reduced expansion rate compared with P0 and P7 myoblasts and an increased tendency to fuse. We thus concluded that myogenic cells derived from the $CD34^{+}ITGA7^{+}$ fraction acquire increasing fusogenicity from birth to adulthood. Such observations are coherent with previous findings showing that the fusion efficiency increases during development and that MuSCs exhibit different properties during fetal development and the adult stage (Biressi et al., 2007; Tierney et al., 2016). Fetal MuSCs were shown to be more resistant to myogenic progression upon *in vitro* expansion and exhibit enhanced regenerative potential *in vivo* but reduced ability to repopulate the muscle niche compared with adult MuSCs (Tierney et al., 2016). Finally, we demonstrated that differences upon *in vitro* culture were merely dependent on the initial pool of PAX7+ cells upon seeding and reflected the different steps of postnatal growth, namely the expansion phase of PAX7+ cells observed in the initial days of postnatal growth (P0–P5), and the waves of myogenic commitment and differentiation observed after P6 and P15. Therefore, we deem that the differential abilities of PAX7+ cells to progress in the myogenic differentiation program during postnatal growth and in adulthood should be taken into consideration for *in vitro* assays as well as for cell-based therapy strategies.

Overall, our study contributes to a better understanding of the progression of the myogenic cells in the differentiation program, and demonstrates that this process is characterized by a complex diversity of myogenic states. In addition, we established the relative proportions of the myogenic populations and their evolution over time, as well as the precise kinetic of quiescent MuSC pool organization during the postnatal growth process.

## EXPERIMENTAL PROCEDURES

### Mice

C57BL/6N mice were purchased from Janvier Labs and bred for postnatal growth study. Animals were handled according to French and European Community guidelines.

## Cell Isolation and Dissociation of Muscle Tissue

Hindlimb muscles deriving from a single mouse were dissected and finely minced in Hank's balanced salt solution (HBSS) (Gibco). Minced muscles were enzymatically digested for 60 min (postnatal muscles) to 90 min (P56 adult muscles) at 37°C with agitation every 20 min in a solution containing collagenase A (2 mg/mL, Roche), dispase II (3 mg/mL, Roche), DNase I (10 μg/mL, Roche), 0.4 mM $CaCl_2$ (Sigma), and 5 mM $MgCl_2$ (Sigma). The resulting cell suspension was washed with HBSS with addition of 0.2% bovine serum albumin (BSA) and 0.5% antibiotics (Gibco) and passed successively through 100- and 40-μm nylon filters (Falcon). Red blood cells were lysed in 1 mL of red blood cell lysing buffer (BD Biosciences) for 20 min. Cells were then transferred to flow cytometry collection tube.

## Purification of MuSCs by FACS

Mononucleated cells from digested muscles were incubated for 45 min on ice with the mix of conjugated antibodies listed in Table S1, and MuSCs were sorted as reported previously (Gromova et al., 2015).

## Cell Culture

FACS-sorted MuSCs were plated at clonal density (400 cells/$cm^2$) on gelatin-coated flasks (Corning) or on gelatin-coated 8-well μ-Slides (ibidi) in DMEM (Gibco) supplemented with 20% fetal bovine serum (HyClone), 10% horse serum (Life Technologies), 5 ng/mL basic fibroblast growth factor (PrepoTech) and 0.5% antibiotics and kept in culture for 3, 4, and 5 days. Fresh medium was added 2 days after seeding.

## Cell Fixation and Immunostaining for Flow Cytometry Analysis

Cells deriving from digested muscles or cultured-myogenic cells were labeled with 1 mL of Fixable Viability Stain 780 (1:1,000, BD Biosciences) in HBSS for 10 min. Cells were washed with HBSS, and then fixed and permeabilized in 500 μL of fixation solution (Transcription Buffer Set, BD Pharmingen) for 45 min at +4°C, accordingly to manufacture instructions. Fixed cells were washed with the permeabilization/wash buffer (Transcription Buffer Set, BD Pharmingen) and proceeded for nuclear immunostaining. Cells were incubated with BSA 5% for 15 min and then with the mix of conjugated antibodies for 50 min at room temperature. The following mix of conjugated antibodies was used: mouse anti-PAX3/7-AF647 (B-5), mouse anti-MYOD-PE coupled using SiteClick PE Antibody Kit (no. S10467, Invitrogen), mouse anti-MYOG-AF488 (5FD), and mouse anti-KI67-bV421. A detailed list of the coupled antibodies and the working dilutions used is provided in Table S3. Cells were washed with the permeabilization/wash solution, re-suspended in HBSS and analyzed using a BD FACSCanto Flow Cytometer (BD Biosciences). For *in vivo* experiments, acquisitions were performed on a mean of 35,000 living cells for postnatal muscles and of 5,000 living cells for adult muscles. For *in vitro* experiments acquisitions were performed on 5,000 to 10,000 living cells.

## IF

Following fixation (4% paraformaldehyde [PFA], 10 min), cultured cells were washed with PBS, permeabilized for 10 min in 0.1% Triton X-100 (Sigma), and blocked with a solution containing 5% BSA (Sigma) and 0.05% Triton X-100 for 1 h at room temperature. Cells were incubated with primary antibodies overnight at 4°C, and then with appropriate coupled secondary antibodies for 1 h at room temperature.

Muscles were dissected and snap frozen in liquid nitrogen-cooled isopentane. Muscle sections (10 μm) were fixed with 4% PFA for 20 min, permeabilized in cold methanol for 6 min, and boiled in citrate buffer (Dako) for epitope retrieval. The blocking was performed for 2 h at room temperature with BSA 5% and then for 30 min with anti-mouse IgG Fab fragment (Jackson Laboratories). A detailed list of the antibodies used is provided in Table S4.

## Image Analysis

For optical analysis, images were acquired using an Olympus CKX41 inverted microscope. For IF analysis, images were acquired using LSM800 confocal microscope (Zeiss). For IF on cross-sections, four fields of view (20×) for P0, P3, P7, P10, and P15, and seven fields of view (20×) for P21, P28, and P56 were acquired per TA muscle.

## Statistic and Reproducibility

Flow cytometry analyses and morphological characterization of *in vitro* expanded cells were performed on three independent experiments. Flow cytometry analyses of digested muscles were performed on at least three to five mice. IF analyses on muscle sections were performed on n = 3 mice. Results are represented as mean ± SEM. Statistical analysis were performed using GraphPad Prism software. Statistical significance was determined by one- and two-way ANOVA tests followed by Tukey's multiple comparisons test. $p < 0.05$ was considered significant (*$p < 0.05$, **$p < 0.01$, ***$p < 0.001$, ****$p < 0.0001$). ns represents statistically not significant.

# SUPPLEMENTAL INFORMATION

Supplemental Information can be found online at https://doi.org/10.1016/j.stemcr.2020.07.011.

# AUTHOR CONTRIBUTIONS

F.G. and N.D. designed the study. F.G., N.D., and B.L. performed the experiments and analyzed the data. F.G., N.D., and F.R. wrote the manuscript. F.R. and H.R. acquired the funding and supplied the resources. N.D. and F.R. supervised and coordinated the study.

# ACKNOWLEDGMENTS

We thank Joel Cassler for proofreading the manuscript, and Catherine Blanc and Bénédicte Hoareau from the Flow Cytometry Platform CyPS (Plateforme de cytométrie CyPS, La Pitié Salpêtrière, Paris) for MuSC sorting. This work was supported by: FR funding from Association Française contre les Myopathies (AFM) via TRANSLAMUSCLE (PROJECT 19507), Agence Nationale de la Recherche (ANR) grant BMP-MyoStem (ANR-16-CE14-0002-03), MyoStemVasc (ANR-17-CE14-0018-01), RHU CARMMA (ANR-15-RHUS-0003), Labex REVIVE (ANR-10-LABX-73), and Etablissement Français du Sang (EFS) dotation.

Received: February 13, 2020
Revised: July 9, 2020
Accepted: July 10, 2020
Published: August 6, 2020

## REFERENCES

Bachman, J.F., Klose, A., Liu, W., Paris, N.D., Blanc, R.S., Schmalz, M., Knapp, E., and Chakkalakal, J.V. (2018). Prepubertal skeletal muscle growth requires PAX7-expressing satellite cell-derived myonuclear contribution. Development *145*, dev167197.

Biressi, S., Molinaro, M., and Cossu, G. (2007). Cellular heterogeneity during vertebrate skeletal muscle development. Dev. Biol. *308*, 281–293.

Bröhl, D., Vasyutina, E., Czajkowski, M.T., Griger, J., Rassek, C., Rahn, H.-P., Purfürst, B., Wende, H., and Birchmeier, C. (2012). Colonization of the satellite cell niche by skeletal muscle progenitor cells depends on notch signals. Dev. Cell *23*, 469–481.

Chakkalakal, J.V., Christensen, J., Xiang, W., Tierney, M.T., Boscolo, F.S., Sacco, A., and Brack, A.S. (2014). Early forming label-retaining muscle stem cells require p27kip1 for maintenance of the primitive state. Development *141*, 1649–1659.

Chargé, S.B.P., and Rudnicki, M.A. (2004). Cellular and molecular regulation of muscle regeneration. Physiol. Rev. *84*, 209–238.

Danoviz, M.E., and Yablonka-Reuveni, Z. (2012). Skeletal muscle satellite cells: background and methods for isolation and analysis in a primary culture system. Methods Mol. Biol. *798*, 21–52.

Eliazer, S., Muncie, J.M., Christensen, J., Sun, X., D'Urso, R.S., Weaver, V.M., and Brack, A.S. (2019). Wnt4 from the niche controls the mechano-properties and quiescent state of muscle stem cells. Cell Stem Cell *25*, 654–665.e4.

Gromova, A., Tierney, M.T., and Sacco, A. (2015). FACS-based satellite cell isolation from mouse hind limb muscles. Bio. Protoc. *5*, e1558.

Gros, J., Manceau, M., Thomé, V., and Marcelle, C. (2005). A common somitic origin for embryonic muscle progenitors and satellite cells. Nature *435*, 954–958.

Kassar-Duchossoy, L., Giacone, E., Gayraud-Morel, B., Jory, A., Gomès, D., and Tajbakhsh, S. (2005). Pax3/PAX7 mark a novel population of primitive myogenic cells during development. Genes Dev. *19*, 1426–1431.

Katz, B. (1961). The termination of the afferent nerve fibre in the muscle spindle of the frog. Philos. Trans. R. Soc. Lond. B Biol. Sci. *243*, 221–240.

Kim, J.-H., Han, G.-C., Seo, J.-Y., Park, I., Park, W., Jeong, H.-W., Lee, S.H., Bae, S.-H., Seong, J., Yum, M.-K., et al. (2016). Sex hormones establish a reserve pool of adult muscle stem cells. Nat. Cell Biol. *18*, 930–940.

Kuang, S., Kuroda, K., Le Grand, F., and Rudnicki, M.A. (2007). Asymmetric self-renewal and commitment of satellite stem cells in muscle. Cell *129*, 999–1010.

Lepper, C., Conway, S.J., and Fan, C.-M. (2009). Adult satellite cells and embryonic muscle progenitors have distinct genetic requirements. Nature *460*, 627–631.

Lepper, C., Partridge, T.A., and Fan, C.-M. (2011). An absolute requirement for PAX7-positive satellite cells in acute injury-induced skeletal muscle regeneration. Development *138*, 3639–3646.

Machado, L., Esteves de Lima, J., Fabre, O., Proux, C., Legendre, R., Szegedi, A., Varet, H., Ingerslev, L.R., Barrès, R., Relaix, F., et al. (2017). In situ fixation redefines quiescence and early activation of skeletal muscle stem cells. Cell Rep. *21*, 1982–1993.

Maesner, C.C., Almada, A.E., and Wagers, A.J. (2016). Established cell surface markers efficiently isolate highly overlapping populations of skeletal muscle satellite cells by fluorescence-activated cell sorting. Skelet. Muscle *6*, 35.

Mauro, A. (1961). Satellite cell of skeletal muscle fibers. J. Biophys. Biochem. Cytol. *9*, 493–495.

McCarthy, J.J., Mula, J., Miyazaki, M., Erfani, R., Garrison, K., Farooqui, A.B., Srikuea, R., Lawson, B.A., Grimes, B., Keller, C., et al. (2011). Effective fiber hypertrophy in satellite cell-depleted skeletal muscle. Development *138*, 3657–3666.

Montarras, D., Morgan, J., Collins, C., Relaix, F., Zaffran, S., Cumano, A., Partridge, T., and Buckingham, M. (2005). Direct isolation of satellite cells for skeletal muscle regeneration. Science *309*, 2064–2067.

Murphy, M.M., Lawson, J.A., Mathew, S.J., Hutcheson, D.A., and Kardon, G. (2011). Satellite cells, connective tissue fibroblasts and their interactions are crucial for muscle regeneration. Development *138*, 3625–3637.

Pala, F., Di Girolamo, D., Mella, S., Yennek, S., Chatre, L., Ricchetti, M., and Tajbakhsh, S. (2018). Distinct metabolic states govern skeletal muscle stem cell fates during prenatal and postnatal myogenesis. J. Cell Sci. *131*, jcs212977.

Paris, N.D., Soroka, A., Klose, A., Liu, W., and Chakkalakal, J.V. (2016). Smad4 restricts differentiation to promote expansion of satellite cell derived progenitors during skeletal muscle regeneration. Elife *5*, e19484.

Pasut, A., Oleynik, P., and Rudnicki, M.A. (2012). Isolation of muscle stem cells by fluorescence activated cell sorting cytometry. Methods Mol. Biol. *798*, 53–64.

Picard, C.A., and Marcelle, C. (2013). Two distinct muscle progenitor populations coexist throughout amniote development. Dev. Biol. *373*, 141–148.

Relaix, F., and Zammit, P.S. (2012). Satellite cells are essential for skeletal muscle regeneration: the cell on the edge returns centre stage. Development *139*, 2845–2856.

Relaix, F., Rocancourt, D., Mansouri, A., and Buckingham, M. (2005). A Pax3/PAX7-dependent population of skeletal muscle progenitor cells. Nature *435*, 948–953.

Rudnicki, M.A., Schnegelsberg, P.N., Stead, R.H., Braun, T., Arnold, H.H., and Jaenisch, R. (1993). MYOD or Myf-5 is required for the formation of skeletal muscle. Cell *75*, 1351–1359.

Sambasivan, R., Yao, R., Kissenpfennig, A., Van Wittenberghe, L., Paldi, A., Gayraud-Morel, B., Guenou, H., Malissen, B., Tajbakhsh, S., and Galy, A. (2011). PAX7-expressing satellite cells are indispensable for adult skeletal muscle regeneration. Development *138*, 3647–3656.

Sato, T., Yamamoto, T., and Sehara-Fujisawa, A. (2014). miR-195/497 induce postnatal quiescence of skeletal muscle stem cells. Nat. Commun. *5*, 4597.

Stantzou, A., Schirwis, E., Swist, S., Alonso-Martin, S., Polydorou, I., Zarrouki, F., Mouisel, E., Beley, C., Julien, A., Le Grand, F., et al. (2017). BMP signaling regulates satellite cell-dependent postnatal muscle growth. Development *144*, 2737–2747.

Tapscott, S.J. (2005). The circuitry of a master switch: MYOD and the regulation of skeletal muscle gene transcription. Development *132*, 2685–2695.

Tierney, M.T., Gromova, A., Sesillo, F.B., Sala, D., Spenlé, C., Orend, G., and Sacco, A. (2016). Autonomous extracellular matrix remodeling controls a progressive adaptation in muscle stem cell regenerative capacity during development. Cell Rep. *14*, 1940–1952.

Verma, M., Asakura, Y., Murakonda, B.S.R., Pengo, T., Latroche, C., Chazaud, B., McLoon, L.K., and Asakura, A. (2018). Muscle satellite cell cross-talk with a vascular niche maintains quiescence via VEGF and notch signaling. Cell Stem Cell *23*, 530–543.e9.

White, R.B., Biérinx, A.-S., Gnocchi, V.F., and Zammit, P.S. (2010). Dynamics of muscle fibre growth during postnatal mouse development. BMC Dev. Biol. *10*, 21.

Wood, W.M., Etemad, S., Yamamoto, M., and Goldhamer, D.J. (2013). MYOD-expressing progenitors are essential for skeletal myogenesis and satellite cell development. Dev. Biol. *384*, 114–127.

Zammit, P.S., Heslop, L., Hudon, V., Rosenblatt, J.D., Tajbakhsh, S., Buckingham, M.E., Beauchamp, J.R., and Partridge, T.A. (2002). Kinetics of myoblast proliferation show that resident satellite cells are competent to fully regenerate skeletal muscle fibers. Exp. Cell Res. *281*, 39–49.

Zammit, P.S., Golding, J.P., Nagata, Y., Hudon, V., Partridge, T.A., and Beauchamp, J.R. (2004). Muscle satellite cells adopt divergent fates: a mechanism for self-renewal? J. Cell Biol. *166*, 347–357.

**Stem Cell Reports, Volume *15***

## Supplemental Information

# Distinct Phases of Postnatal Skeletal Muscle Growth Govern the Progressive Establishment of Muscle Stem Cell Quiescence

**Francesca Gattazzo, Béatrice Laurent, Frédéric Relaix, Hélène Rouard, and Nathalie Didier**

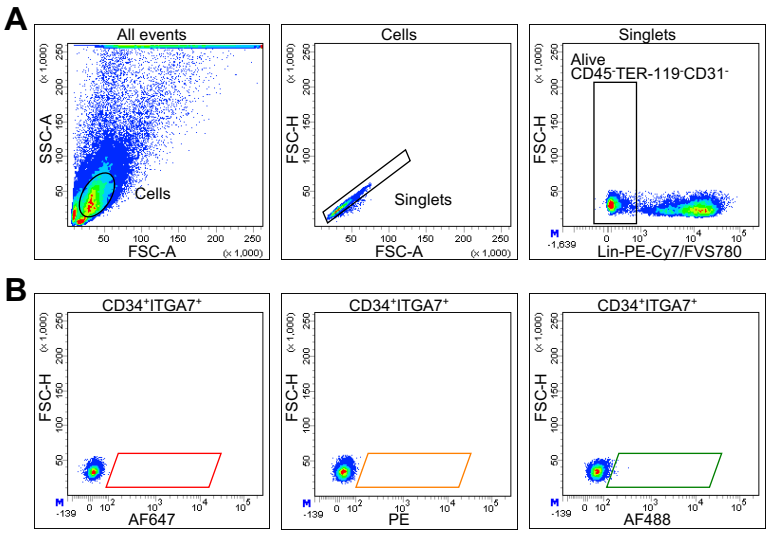


**Figure S1. Characterization and purification of CD34$^+$ITGA7$^+$ myogenic fraction from postnatal and adult hind-limb muscles. Related to Figure 1.** Strategy for determining the proportion of PAX7+, MYOD+, MYOG+ cells among the CD45$^-$TER-119$^-$CD31$^-$SCA-1$^-$CD34$^+$ITGA7$^+$ fraction (referred to as CD34$^+$ITGA7$^+$ fraction). Representative density scatterplots showing the gates used to analyse CD34$^+$ITGA7$^+$ fraction from P7 mouse muscles. (**A**) Debris, doublets, Lin+ cells (namely, CD45$^+$TER-119$^+$CD31$^+$ cells) and dead cells were excluded from the analysis. (**B**) Fluorescence Minus One controls (FMO) gates were used to determine the positivity for PAX7+, MYOD+, MYOG+ cells among the CD34$^+$ITGA7$^+$ fraction.

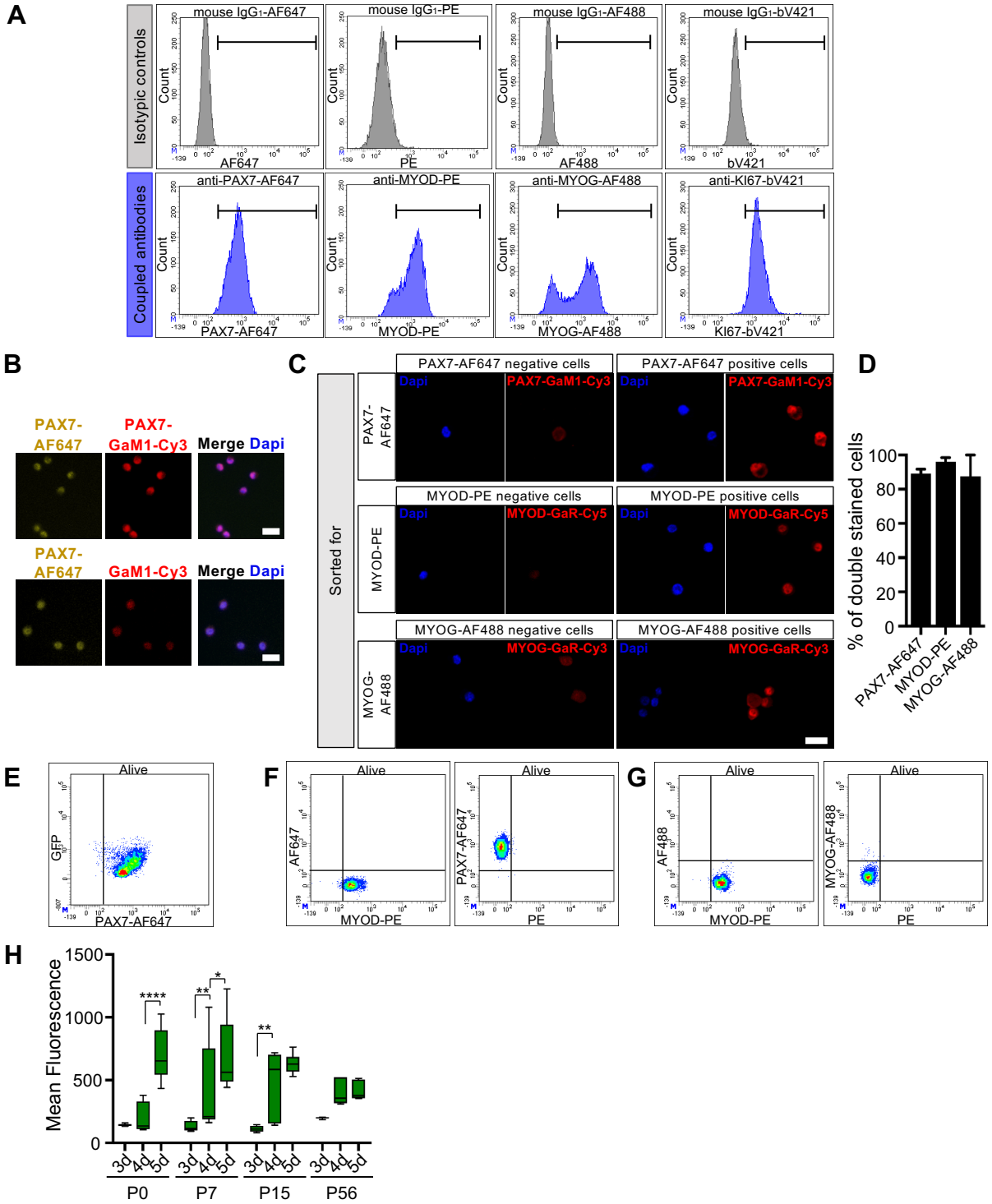


**Figure S2. Validation of the coupled antibodies used for flow cytometry analysis of cultured myogenic cells. Related to Figure 2.** (**A**) Cells were stained with the coupled isotypic control immunoglobulin or the coupled antibody at the same concentration. (**B-D**) Cells immunostained with coupled antibodies were FACS sorted and counterstained with distinct primary antibodies. See Supplemental Experimental Procedure. (**B**) Images showing the different intensity of the signal when cells immunostained with coupled anti-PAX7-AF647 (#sc-365843) were counterstained with primary mouse anti-PAX7 (#sc-81648) and secondary GaM1-Cy3 antibodies or with secondary GaM1-Cy3 antibody only. Only cells with a strong signal intensity were considered as double stained for PAX7. (**C**) Representative images of FACS sorted cells counterstained for PAX7, MYOD and MYOG. Scale bar, 25 µm. (**D**) Percentage of double stained cells. Data are shown as mean ± SEM of replicates (n=1 experiment). (**E**) Density scatter plot showing the correlation between endogenous PAX7 expression revealed with coupled anti-PAX7-AF647 antibody and GFP transgene expression in cultured cells derived from *Tg:Pax7-nGFP* mouse muscles. (**F-G**) Fluorescence Minus One (FMO) controls used to position the gates on Figure 2. (**H**) Mean level of expression of MYOG in mononucleated cells cultured for 3, 4 and 5 days determined by flow cytometry. Values are the mean ± SEM of 3 independent experiments. Two-Way ANOVA analysis, with **p<0.05, **p<0.01, ****p<0.0001*.

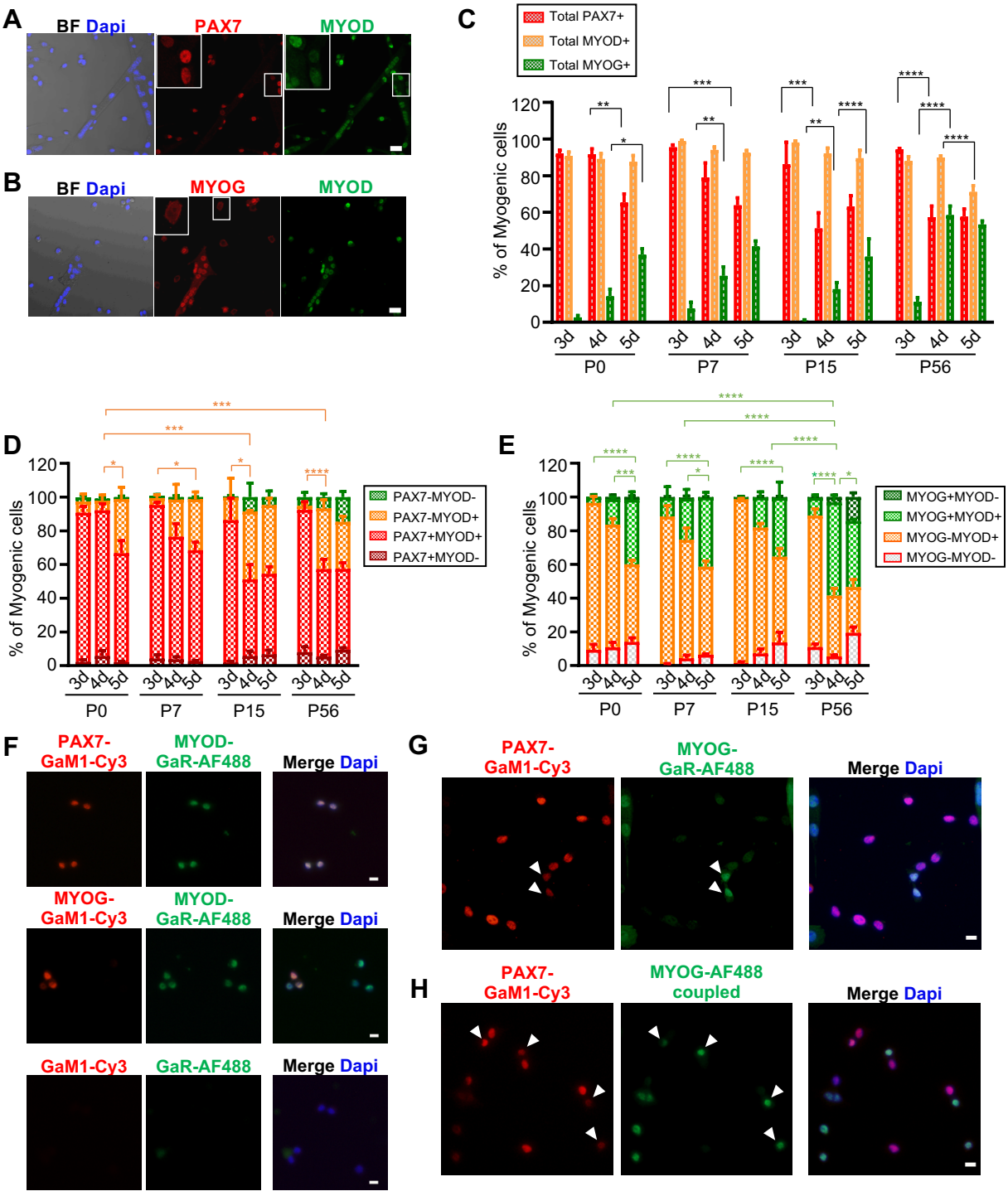


**Figure S3. Analysis of the *in vitro* behavior of myogenic cells of the CD34$^{+}$ITGA7$^{+}$ fraction by immunofluorescence. Related to Figure 2.** (**A, B**) Representative images of cells stained for (**A**) PAX7 (red) and MYOD (green) and (**B**) MYOD (green) and MYOG (red). Nuclei were stained with DAPI. Magnification inlets show the variability of intensity of fluorescence signal. Scale bar, 20 µm. Graphs showing, (**C**) the quantification of the proportion of total PAX7+, MYOD+ and MYOG+ cells on the total myogenic population, (**D**) the distribution of PAX7 and MYOD, (**E**) the distribution of MYOD and MYOG on the total myogenic population. Values are represented as the mean ± SEM from 3 independent experiments (n=3 mice per group). Only mononucleated cells were quantified. Minimum 7 fields (20x) per well were quantified. (**F**) Representative images of cells immunostained for PAX7 (red) and MYOD (green) or MYOD (green) and MYOG (red) and the corresponding negative controls incubated with the secondary antibodies only. (**G, H**) Representative images of P56 cells cultured for 5 days in GM showing the co-expression of PAX7 and MYOG. Cells were immunostained for PAX7 (red) (#sc-81648) and MYOG (green) using (**G**) a rabbit anti-MYOG antibody (#sc-576), or (**H**) a coupled mouse anti-MYOG-AF488 antibody (#sc-52903). See Supplemental experimental procedures. Arrowheads point to double positive PAX7+MYOG+ cells. Scale bar, 20 µm.

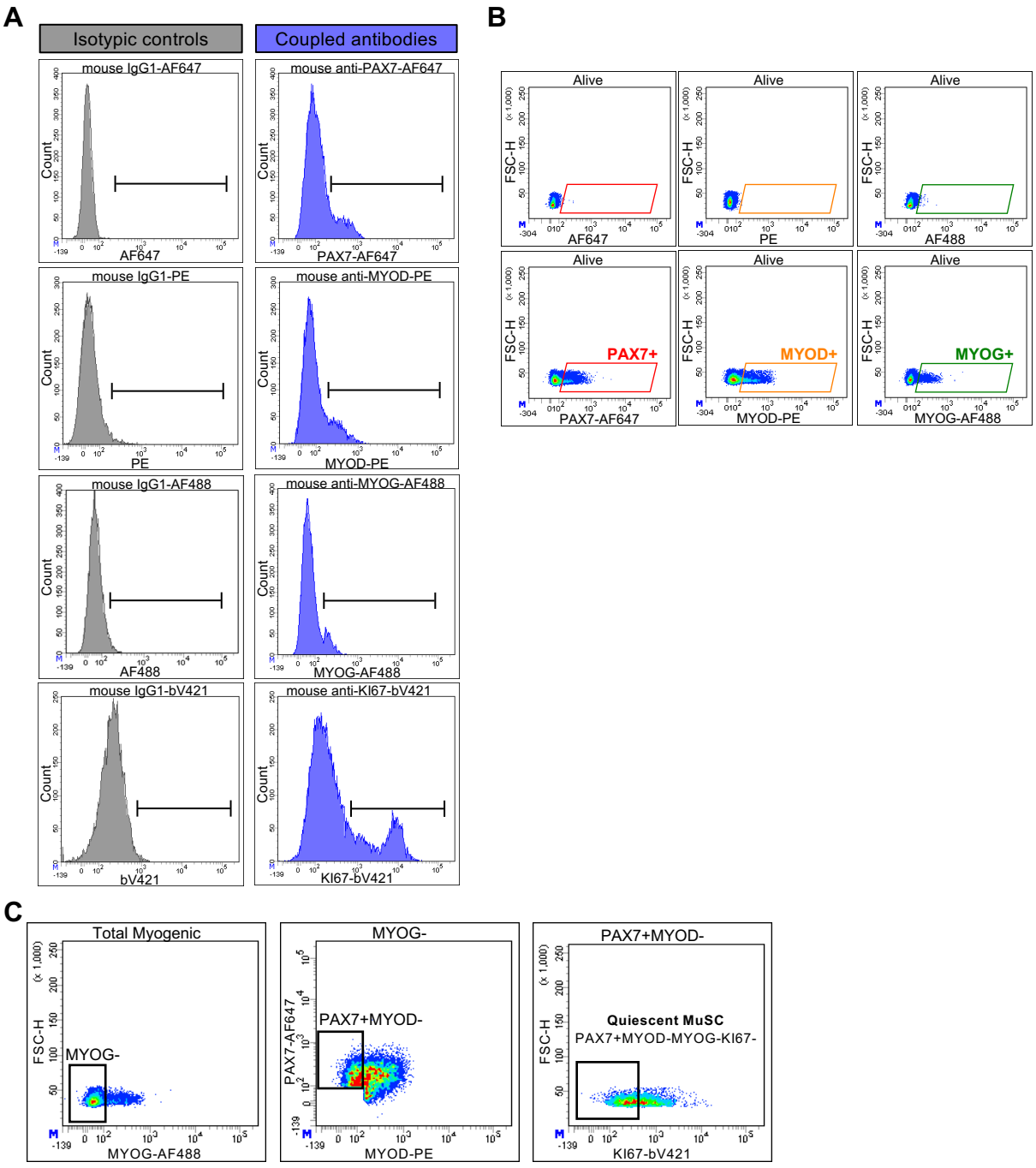


**Figure S4. Validation of the *in vivo* flow cytometry analysis. Related to Figure 3.** (**A**) Specificity of mouse coupled antibodies used for the *in vivo* analysis by flow cytometry. Mononucleated cells from P7 digested muscles were stained with either the coupled isotypic control immunoglobulin, either the mouse coupled antibody. (**B**) FMO controls used to position the gates for PAX7, MYOD and MYOG positivity. (**C**) Representative density scatterplots showing the gating strategy used to select quiescent MuSC defined as the PAX7+MYOD-MYOG-KI67- fraction.

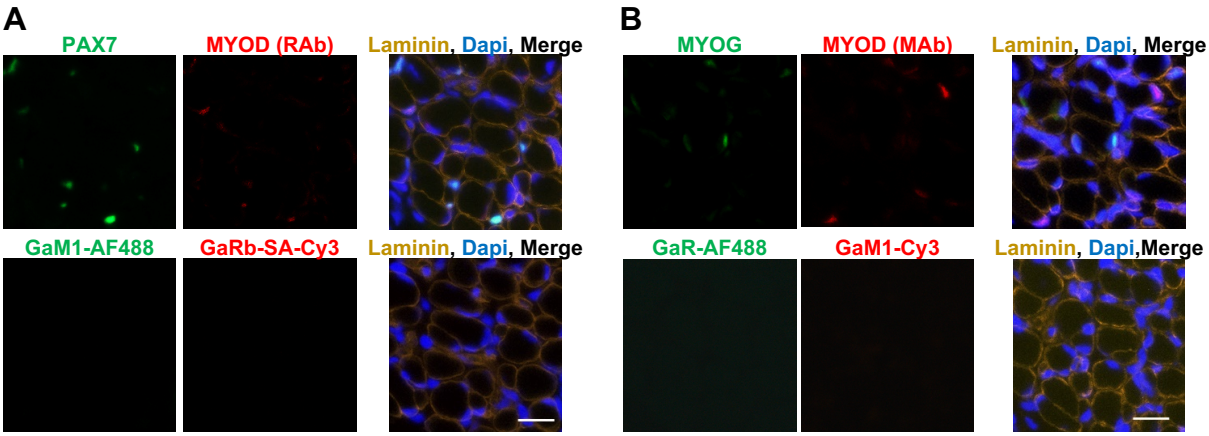


**Figure S5. Validation of the immunostaining protocol on muscle sections. Related to Figure 4.** Representative tibialis anterior (TA*)* muscle cross-sections of P3 mouse immunostained for (**A**) PAX7 (green), MYOD (red) (upper panel), or corresponding secondary antibodies only: GaM1-AF488 for Goat anti-Mouse IgG1-AF488 and GaRb-SA-Cy3 for Goat anti-Rabbit biotinylated-Streptavidin-Cy3 (bottom panel), (**B**) MYOG (green), MYOD (red) (upper panel), or corresponding secondary antibodies only: GaR-AF488 for Goat anti-Rabbit-AF488 and GaM1-Cy3 for Goat anti-Mouse IgG1-Cy3 (bottom panel). Laminin was immunostained (yellow) in each panel. Nuclei were stained with DAPI. Scale bar, 20 μm.

## Supplemental Tables

**Table S1. List of antibodies used for sorting and analysis of MuSC by flow cytometry. Related to Figure 1.**

| Protein | Catalog | Dilution** | Brand |
|---|---|---|---|
| rat anti-mouse CD45-PECy7 | #552848 | 1 µg/300 µl | BD Biosciences |
| rat anti-mouse TER-119-PECy7 | #557853 | 1 µg/300 µl | BD Biosciences |
| rat anti-mouse CD31-PE-Cy7 | #561410 | 1 µg/300 µl | BD Biosciences |
| rat anti-mouse CD34-bV421 | #562608 | 1 µg/300 µl | BD Biosciences |
| rat anti-mouse SCA-1-FITC | #553335 | 1 µg/300 µl | BD Biosciences |
| rat anti-mouse SCA-1-PE | #553108 | 1 µg/300 µl | BD Biosciences |
| mouse anti-mouse ITGA7-AF700 | #FAB3518N | 0.2 µg/300 µl | R&D Systems |
| mouse anti-mouse ITGA7-FITC | #NBP154412 | 1 µg/300 µl | Novus |

**Amount of antibodies used for the immunostaining of mononucleated cells from digested hind-limb muscles of one adult mouse.

**Table S2. Mean fold increase number of mononucleated cells between 3 and 5 days of culture. Related to Figure 1.**

| | Mean fold increase 5d *vs* 3d |
|---|---|
| P0 | 8.7 |
| P7 | 3.9 |
| P15 | 3.8 |
| P56 | 4.0 |

**Table S3. List of antibodies used for nuclear factors immunostaining for flow cytometry analysis. Related to Figure 2.**

| Protein | Catalog | Dilution* | Brand |
|---|---|---|---|
| mouse anti-PAX3/7-AF647 (B-5) | #sc-365843 | 20 ng/100 µl | Santa Cruz |
| mouse anti-MYOG-AF488 (5FD) | #sc-52903 | 20 ng/100 µl | Santa Cruz |
| mouse anti-MYOD-PE | #554130 | 80 ng/100 µl | BD Biosciences |
| mouse anti-KI67-bV421 | #562899 | 4.5 µl/100 µl | BD Biosciences |
| mouse IgG1-AF647 | #sc-24636 | 20 ng/100 µl | Santa Cruz |
| mouse IgG1-AF488 | #sc-3890 | 20 ng/100 µl | Santa Cruz |
| mouse IgG1-PE | #550617 | 80 ng/100µl | BD Biosciences |
| mouse IgG1-bV421 | #562438 | 4.5 µl/100 µl | BD Biosciences |

*Amount of antibodies used for the immunostaining of $2.10^5$ mononucleated cells from digested muscles.

**Table S4. List of antibodies used for IF staining. Related to Figure 2.**

| Protein | Catalog | Final Dilution | Brand |
|---|---|---|---|
| mouse IgG1 anti-PAX7 | #sc-81648 | 1:100 | Santa Cruz (same as DSHB Ab) |
| mouse IgG1 anti-MYOD (MAb) | #554130 | 1:100 | BD Biosciences |
| mouse IgG1 anti-MYOG 5FD | #sc-52903 | 1:100 | Santa Cruz |
| rabbit anti-MYOD M-318 (RAb) | #sc-760 | 1:100 | Santa Cruz |
| rabbit anti-MYOG M-225 | #sc-576 | 1:100 | Santa Cruz |
| rabbit anti-KI67 D3B5 | #9129 | 1:150 | Cell Signaling |
| rabbit anti-Laminin | #L9393 | 1:200 | Sigma |
| | | | |
| **Secondary antibodies** | **Catalog** | **Final Dilution** | **Brand** |
| Goat anti-Mouse IgG1-AF488 (GaM1-AF488) | #115-545-205 | 1:800 | Jackson Immunoresearch |
| Goat anti-Mouse IgG1-Cy3 (GaM1-Cy3) | #115-165-205 | 1:800 | Jackson Immunoresearch |
| Goat anti-Rabbit-AF488 (GaR-AF488) | #111-545-144 | 1:800 | Jackson Immunoresearch |
| Goat anti-Rabbit-Cy3 (GaR-Cy3) | #111-165-144 | 1:800 | Jackson Immunoresearch |
| Goat anti-Rabbit-Cy5 (GaR-Cy5) | #A10523 | 1:800 | Jackson Immunoresearch |
| Goat anti-Rabbit IgG biotin (GaRb) | #111-065-144 | 1:1000 | Jackson Immunoresearch |
| Streptavidin-Cy3 (SA-Cy3) | #016-160-084 | 1:1250 | Jackson Immunoresearch |
| Goat anti-mouse immunoglobulin G (IgG) Fab fragment | #115-007-003 | 1:100 | Jackson Immunoresearch |

**Table S5. Statistical analysis of the global repartition of myogenic cells and PAX7/MYOD and MYOD/MYOG repartition on Total Myogenic cells. Related to Figures 3E, 3F and 3G.**

| Two Way ANOVA **Fig. 3E** | **Total PAX7+** | **Total MYOD$^+$** | **Total MYOG$^+$** | |
|---|---|---|---|---|
| P0 *vs* P3/P4 | ns | ns | ns | |
| P0 *vs* P5/P6 | *,** | ns | ns | |
| P0 *vs* P7-P10 | **,*** | ns | ns | |
| P0 *vs* P15 | * | ns | ns | |
| P0 *vs* P21, P28 | ns | ns | ns | |
| P0 *vs* P49 | ns | **** | ns | |
| P0 *vs* P56 | *** | **** | ** | |
| P7/P8 *vs* P10/P15 | ns | ns | ns | |
| P10 *vs* P15 | ns | ns | ns | |
| P10 *vs* P21 | ns | * | ** | |
| P15 *vs* P21 | ns | ns | ns | |
| P7 *vs* P49/P56 | **** | **** | **/**** | |
| P10 *vs* P49/P56 | **** | **** | ***/**** | |
| P15 *vs* P49/P56 | **** | **** | ns/*** | |
| P21 *vs* P49/P56 | **** | **** | ns | |
| P21 *vs* P28 | ns | ** | ns | |
| P28 *vs* P49 | * | **** | ns | |
| P28 *vs* P56 | **** | **** | * | |
| P49 *vs* P56 | ns | ns | ns | |
| **Fig. 3F** | **PAX7$^+$ MYOD$^-$** | **PAX7$^+$ MYOD$^+$** | **PAX7$^-$ MYOD$^+$** | **PAX7$^-$ MYOD$^-$** |
| P0 *vs* P3/P4 | ns | ns | ns | ns |
| P0 *vs* P5/P6 | ns | **** | **,*** | ns |
| P0 *vs* P7/P8 | ns | **,ns | ns | ns |
| P0 *vs* P10/15 | ns | ****,* | * | ns |
| P0 *vs* P21 | ns | ns | * | ns |
| P0 *vs* P28 | ns | ns | ns | ns |
| P0 *vs* P49/P56 | **** | **** | ns,** | ns |
| P3/P4 *vs* P6 | ns | ***,** | ns | ns |
| P3/P4 *vs* P49/P56 | **** | **** | **** | ns |
| P6 *vs* P49/P56 | **** | ns | **** | ns |
| P7/P8/P10 *vs* P15 | ns | ns | ns | ns |
| P7 *vs* P21 | ns | ns | ns | * |
| P7/P10 *vs* P49 | **** | ns | ***,**** | * |
| P7/P10 *vs* P56 | **** | *,ns | **** | **** |
| P8 *vs* P49/P56 | **** | **,**** | **** | ns,* |
| P10 *vs* P21 | ns | * | ns | ns |
| P15 *vs* P21 | ns | ns | ns | ns |
| P15/P21 *vs* P28 | ** | ns | ** | ns |
| P15/P21 *vs* P49 | **** | *,**** | **** | ns |
| P15/P21 *vs* P56 | **** | ***,**** | **** | ns |
| P28 *vs* P49 | **** | *** | ns | ns |
| P28 *vs* P56 | **** | **** | *** | ns |
| P49 *vs* P56 | * | ns | ns | ns |
| **Fig. 3G** | **MYOG$^+$ MYOD$^-$** | **MYOG$^+$ MYOD$^+$** | **MYOG$^-$ MYOD$^+$** | **MYOG$^-$ MYOD$^-$** |
| P0 *vs* P3-P15 | ns | ns | ns | ns |
| P0 *vs* P21 | ns | ns | * | ns |
| P0 *vs* P28 | ns | ns | ns | ns |
| P0 *vs* P49 | ns | ns | **** | **** |
| P0 *vs* P56 | ns | * | **** | **** |
| P3 *vs* P7 | * | ns | ns | ns |
| P3 *vs* P10 | * | ns | ** | ns |
| P6 *vs* P49/P56 | ns | ns | **** | **** |
| P7/P8/P10 *vs* P15 | ns | ns | ns | ns |
| P7 *vs* P21 | * | ns | *** | ns |

| | | | | |
|---|---|---|---|---|
| P8 *vs* P49/P56 | ns,** | ns | **** | **** |
| P10 *vs* P21 | * | ns | **** | ns |
| P7/P10 *vs* P49 | * | ns | **** | **** |
| P7/P10 *vs* P56 | **** | ns,* | **** | **** |
| P15 *vs* P21 | ns | ns | ns | ns |
| P15 *vs* P28 | ns | ns | ns | ** |
| P21 *vs* P28 | ns | ns | **** | ** |
| P15/P21 *vs* P49/P56 | ns | ns | **** | **** |
| P28 *vs* P49 | ns | ns | **** | **** |
| P49 *vs* P56 | ns | ns | ns | * |

**Table S6. Statistical analysis of the distribution of cycling and non-cycling myogenic populations. Related to Figure 3I.**

| Two Way ANOVA | **Quiescent MuSC** | **Cycling MuSC** | **Cycling PAX7+MYOD+** | **Non-Cycling PAX7+MYOD+** | **Cycling MYOD+** | **Non-Cycling MYOD+** | **MYOG+** |
|---|---|---|---|---|---|---|---|
| P0 *vs* P3/P4 | ns | ns | ns | ns | ns | ns | ns |
| P0 *vs* P5 | ns | ns | ** | ns | **** | ns | ns |
| P0 *vs* P6 | ns | ns | **** | ns | ns | **** | ns |
| P0 *vs* | ns | ns | ** | ns | ns | ns | ns |
| P0 *vs* P10 | ns | ns | *** | ns | ** | ns | ns |
| P0 *vs* P21 | ns | ** | ** | ns | ns | **** | ns |
| P0 *vs* P28 | **** | ns | ** | ns | ns | ns | ns |
| P0 *vs* P49 | **** | ns | **** | ns | ns | ns | ** |
| P0 *vs* P56 | **** | **** | **** | ns | ns | ns | **** |
| P3/P4 *vs* P49 | **** | **,* | **** | ns | ns | ns | ns,** |
| P3/P4 *vs* P56 | **** | **** | **** | ns | *,** | ns | **,**** |
| P5 *vs* P6 | ns | ns | ns | ns | * | **** | ns |
| P5/P6 *vs* P49 | **** | *,ns | *,ns | ns | ****,ns | ns,**** | **,ns |
| P5 *vs* P56 | **** | **** | ** | ns | **** | ns | **** |
| P6 *vs* P7/P10 | ns | ns | ns | ns | ns | **** | **** |
| P6 *vs* P15 | ns | ns | ns | ns | ns | *** | ns |
| P6 *vs* P21 | ns | ** | ns | * | ns | ns | ns |
| P6 *vs* P56 | **** | **** | ns | ns | ns | **** | ** |
| P7 *vs* P8 | ns | ns | ns | ns | ns | ns | ns |
| P7/P8 *vs* P15 | ns | ns | ns | ns | ns | ns | ns |
| P7 *vs* P21 | ns | ns | ns | ns | ns | *** | **** |
| P7/P8 *vs* P49 | **** | ns | ns | ns | ns | ns,* | **** |
| P7/P8 *vs* P56 | **** | ns | ns | ns | **,ns | ns,*** | **** |
| P10 *vs* P15 | ns | ns | ns | ns | ns | ns | ns |
| P10 *vs* P21 | ns | ns | ns | * | * | **** | **** |
| P10 *vs* P49 | **** | ns | ns | ns | **** | ns | **** |
| P10 *vs* P56 | **** | * | ns | ns | **** | ns | **** |
| P15 *vs* P21 | ns | ns | ns | ns | ns | ** | * |
| P15/P21 *vs* P28 | ****/** | ns | ns | ns | ns | ns,**** | ns |
| P15 *vs* P49 | **** | ns | ns | ns | * | ns | *** |
| P15 *vs* P56 | **** | ns | ns | ns | ** | ** | **** |
| P21 *vs* P49 | **** | ns | ns | *** | ns | **** | ns |
| P21 *vs* P56 | **** | ns | * | **** | ns | **** | ** |
| P28 *vs* P49 | **** | ns | ns | ns | ns | ns | ns |
| P28 *vs* P56 | **** | ns | ns | ns | ns | ns | **** |
| P49 *vs* P56 | **** | ns | ns | ns | ns | ns | ns |

**Table S7. Statistical analysis of the repartition of MYOD+ and KI67+ cells among total PAX7+ cells. Related to Figure 5F.**

| Two Way ANOVA | Quiescent MuSC | Cycling MuSC | Non-cycling PAX7+MYOD+ | Cycling PAX7+MYOD+ |
|---|---|---|---|---|
| P0 *vs* P3/P4 | ns | ns | ns | ns |
| P0 *vs* P5 | *** | ns | ns | *** |
| P0 *vs* P6 | **** | ns | ns | **** |
| P0 *vs* P7-P15 | **** | ns | ns | ***,**** |
| P0 *vs* P21 | **** | **** | * | **** |
| P0 *vs* P28 | **** | ns | ns | **** |
| P0 *vs* P49 | **** | *** | ** | ***** |
| P0 *vs* P56 | **** | **** | *** | ***** |
| P3/P4/P5 *vs* P49/P56 | **** | **** | ns | **** |
| P4 *vs* P5 | ns | ns | ns | ** |
| P5 *vs* P6 | * | ns | ns | *** |
| P6 *vs* P7 | ns | *** | ns | * |
| P6 *vs* P8 | ns | **** | *** | ** |
| P6 *vs* P49/P56 | **** | **** | ns | ns |
| P7 *vs* P8 | ns | ns | ns | ns |
| P7/P8 *vs* P15 | ns | ns | ns | ns |
| P7 *vs* P21 | ns | * | *** | ns |
| P7 *vs* P49 | **** | * | ns | *** |
| P7 *vs* P56 | **** | **** | * | **** |
| P8 *vs* P49 | **** | ns | **** | **** |
| P8 *vs* P56 | **** | **** | **** | **** |
| P10 *vs* P15 | ns | ns | * | ns |
| P10 *vs* P21 | ns | **** | **** | ns |
| P10 *vs* P49 | **** | *** | ns | **** |
| P10 *vs* P56 | **** | **** | ns | **** |
| P15 *vs* P21 | ns | ns | ns | ns |
| P15 *vs* P28 | ** | ns | ns | ns |
| P15/P21 *vs* P49 | **** | ns | **** | ***,**** |
| P15 *vs* P56 | **** | **** | **** | **** |
| P21 *vs* P28 | * | ns | *** | ns |
| P21 *vs* P56 | **** | ns | **** | **** |
| P28 *vs* P49 | **** | ns | ns | ns |
| P28 *vs* P56 | **** | ** | * | ** |
| P49 *vs* P56 | ns | ns | ns | ns |

## Supplemental Experimental Procedures

**Validation of the coupled antibodies used for flow cytometry analysis. Related to Figure S2B-D.** $CD45^-TER\text{-}119^-CD31^-SCA\text{-}1^-CD34^+ITGA7^+$ myogenic cells were purified from P7 mouse muscles, plated on gelatin-coated dish and expanded for 4 days in GM. After trypsinization, cells were fixed and permeabilized. Fixed cells were then divided into 3 tubes and respectively immunostained with the coupled antibodies anti-PAX7-AF647 or anti-MYOD-PE or anti-MYOG-AF488 (see **Table S3**) and FACS sorted. The positive and negative fractions were cytospun and immunostained with antibodies commonly used in the field for immunofluorescence from different species except for PAX7: namely mouse IgG1 anti-PAX7 (sc-81648), rabbit anti-MYOD M-318 (sc-760) and rabbit anti-MYOG M-225 (sc-576) (see **Table S4**). Cells were incubated overnight at 4°C with the relative primary antibody of interest. Then, cells were washed with PBS and incubated with the appropriate secondary antibodies (**Table S4**) for 1 hour at room temperature. Nuclei were stained with DAPI. Cells were mounted on microscopy slides with Fluoromount-G. Images were acquired with Zeiss LSM 800 confocal microscope at 20x magnification. For each myogenic marker, the number of double-positive cells was quantified and expressed as percentage. At least 50 cells were quantified per condition.

**Co-immunostaining of PAX7 and MYOG on myogenic cells cultured for 5 days in GM**. **Related to Figure S3H.** Cells were fixed, permeabilized and then incubated for one hour with BSA 5%. Cells were then incubated with primary anti-PAX7 antibody (sc-81648) for 1 hour, washed 3 times with PBS and incubated with secondary GaM1-Cy3 antibody for 1 hour. Cells were then washed 3 times with PBS, and incubated 1 hour with coupled anti-MYOG-AF488 antibody (sc-52903, Santa Cruz). Nuclei were stained with DAPI.